



SYNTHESIS AND CHARACTERIZATION OF $YBa_2Cu_3O_{7-\delta}$ (YBCO)
ADDED BLACK PHOSPHORUS VIA SOLID-STATE REACTION

This report is submitted in accordance with requirement of the Universiti Teknikal Malaysia Melaka (UTeM) for Bachelor Degree of Manufacturing Engineering (Hons)



By

GOH SHI MING

FACULTY OF MANUFACTURING ENGINEERING


2022

DECLARATION

I hereby, declared that this report entitled “Synthesis and Characterization of $YBa_2Cu_3O_{7-\delta}$ (YBCO) Added Black Phosphorus via Solid-State Reaction” is the results of my own research except as cited in reference.



Signature

: 

Author's Name

: GOH SHI MING

Date

: 28th June 2022

APPROVAL

This report is submitted to the Faculty of Manufacturing Engineering of Universiti Teknikal Malaysia Melaka as a partial fulfillment of requirements for the degree of Bachelor of Manufacturing Engineering (Hons.)

The members of supervisory committee are as follow:



(Dr. Mohd Shahadan Bin Mohd Suan)

ABSTRAK

Superkonduktor ialah bahan yang mencapai superkonduktiviti iaitu keadaan jirim yang tiada rintangan elektrik dan tiada medan magnet boleh melaluinya. Dalam kebanyakan kes, superkonduktiviti hanya boleh dicapai pada suhu yang sangat rendah. Superkonduktor suhu tinggi $YBa_2Cu_3O_{7-\delta}$ dengan Fosforus Hitam ditambah telah disintesis melalui tindak balas keadaan pepejal. Kebaharuan kerja penyelidikan ini ialah kaedah tindak balas keadaan pepejal menggunakan kurang tenaga berbanding kaedah sintesis lain untuk memproses superkonduktor $YBa_2Cu_3O_{7-\delta}$ dan menghasilkan pengedaran telaga nanozarah Fosforus Hitam. Tindak balas automatik-pembakaran mengubah gel sitrat-nitrat prekursor yang dirumus menjadi produk abu halus. Ia menghasilkan fasa $YBa_2Cu_3O_{7-\delta}$ selepas proses pengkalsinan yang selanjutnya dirawat haba untuk mencapai superkonduktiviti. Kesan komposisi berbeza Fosforus Hitam ditambah $YBa_2Cu_3O_{7-\delta}$ pada struktur dan sifat superkonduktor $YBa_2Cu_3O_{7-\delta}$ telah disiasat dan dinilai. Kerja ini menunjukkan bahawa tindak balas keadaan pepejal adalah kaedah yang berkesan untuk memperkenalkan Fosforus Hitam sebagai zarah nano yang diedarkan secara homogen dalam superkonduktor $YBa_2Cu_3O_{7-\delta}$.

ABSTRACT

A superconductor is a substance that achieves superconductivity which is a state of matter that is no electrical resistance and no magnetic fields may pass through it. In most cases, superconductivity can only be attained at extremely low temperatures. In this study, the high temperature superconductor $YBa_2Cu_3O_{7-\delta}$ with added Black Phosphorus was synthesized via solid-state reaction. The novelty of this research work is the solid-state reaction method consumed less energy compared with other synthesis methods for processing $YBa_2Cu_3O_{7-\delta}$ superconductor and produced well distribution of Black Phosphorus nanoparticles. The auto-combustion reaction transformed the formulated precursor citrate-nitrate gel into fines ashes product. It yielded $YBa_2Cu_3O_{7-\delta}$ phases after calcination process which was further heat treated to achieve superconductivity. The effects of different compositions of Black Phosphorus added $YBa_2Cu_3O_{7-\delta}$ on the structural and superconducting properties of $YBa_2Cu_3O_{7-\delta}$ were investigated and appraised. This work shows that the solid-state reaction is an effective method to introduce Black Phosphorus as nanoparticles homogeneously distributed in the $YBa_2Cu_3O_{7-\delta}$ superconductor.

DEDICATION

Only

My beloved father, Goh Wai Keong

My appreciated mother, Leow Mei Pin

My adored brother, Goh Chun Kit

For giving me moral support, money, cooperation, encouragement and also understandings

Thank you so much & Love You All Always.

اونيورسيتي تيكنيكل مليسيا ملاك

UNIVERSITI TEKNIKAL MALAYSIA MELAKA

ACKNOWLEDGEMENT

I would like to acknowledge and give my warmest thanks to my supervisor, Dr Mohd Shahadan Bin Mohd Suan who made this work possible. His guidance and advice carried me through all the stages of my project.

I would also like to give special thanks to my family for their continuous support and understanding in completing this report. Last but not least, I would like to give a special thanks to my friends who gave me much motivation and they had given their critical suggestion throughout my research. Thanks for the great friendship.

Finally, I would like to thank everybody who was important to this FYP report, as well as expressing my apology that I could not mention personally each one of you.

TABLE OF CONTENTS

Abstrak	I
Abstract	ii
Dedication	iii
Acknowledgement	iv
Table of Contents	v
List of Tables	vi
List of Figures	vii
List of Abbreviations	ix
CHAPTER 1 INTRODUCTION	1
1.1 Background of Study	1
1.2 Problem Statement.....	2
1.2 Objectives	5
1.3 Scope of Work.....	5
1.4 Significance of Study	6
1.5 Organization of Report	6
1.6 Summary.....	6
CHAPTER 2 LITERATURE REVIEW	7
2.1 A Brief History of Superconductivity	7
2.2 Zero Resistance in Superconductors	10

2.3	Meissner Effect.....	12
2.4	Theory of Superconductivity	13
2.4.1	London Theory	13
2.4.2	Ginzburg-Landau Theory	15
2.5	Flux Pinning in Type II Superconductors	16
2.6	YBCO Superconductor.....	17
2.7	Addition of Nanoparticles in $YBa_2Cu_3O_{7-\delta}$	18
2.8	Black Phosphorus	20
2.9	Solid-State Reaction	22
CHAPTER 3 METHODOLOGY		23
3.1	Materials	23
3.2	Samples Preparation	24
3.2.1	$YBa_2Cu_3O_{7-\delta}$ Samples Preparation	24
3.2.2	Auto- Combustion of the Gel	26
3.2.3	Calcination Process	27
3.2.4	Black Phosphorus Added $YBa_2Cu_3O_{7-\delta}$ Samples	29
3.2.5	Sintering Process	29
3.2.6	Process Flow Chart.....	32
3.3	Characterization Technique	33
3.3.1	X-ray Diffraction (XRD).....	33
3.3.2	Scanning Electron Microscope (SEM).....	35
3.3.3	Resistivity-Temperature (R-T) Measurement by Four-Point Probe	36
CHAPTER 4 RESULTS AND DISCUSSION		38
4.1	Structural Properties of $YBa_2Cu_3O_{7-\delta}$	38
4.2	Microstructure of Black Phosphorus added $YBa_2Cu_3O_{7-\delta}$	43
4.3	Superconducting Properties of $YBa_2Cu_3O_{7-\delta}$	47
CHAPTER 5 CONSLUSION AND RECOMMENDATION		50
5.1	Recommendation	50



اونيورسيتي تيكنيكل مليسيا ملاك

UNIVERSITI TEKNIKAL MALAYSIA MELAKA

LIST OF TABLES

Table 3.1 Raw materials used to prepare stock Solutions	24
Table 3.2 Amount of Materials.....	25
Table 3.3 Amount of Black Phosphorus added into $YBa_2Cu_3O_{7-\delta}$	29



LIST OF FIGURES

Figure 1.1 Armchair structure of 2D Black Phosphorus.....	4
Figure 2.1 Illustration of Kamerlingh Onnes' discovery of superconductivity	9
Figure 2.2 Superconductive Elements in Periodic Table.....	9
Figure 2.3 History of some of the Superconducting Compounds.....	10
Figure 2.4 Schematic B-T phase diagram for Type I superconductors	12
Figure 2.5 Schematic B-T phase diagram for Type II superconductors	13
Figure 2.6 Forces of pinning centre distributed randomly.....	17
Figure 2.7 Structure of $YBa_2Cu_3O_{7-\delta}$ superconductor.....	18
Figure 3.1 $Y(NO_3)_3 \cdot 6H_2O$	25
Figure 3.2 $Ba(NO_3)_2$	25
Figure 3.3 $Cu(NO_3)_2 \cdot 3H_2O$	26
Figure 3.4 $C_6H_8O_7$	26
Figure 3.5 Mixture Solution Placed on Hot Plate	26
Figure 3.6 Physical Appearance of Samples; (a) Mixture Solution, (b) Solution turned Gel, (c) Flammable Combustion, (d) Fine Ashes Product.....	27
Figure 3.7 Resultant Powders Before Calcination	28
Figure 3.8 Resultant Powders After Calcination	28
Figure 3.9 Pelletized Machine	30
Figure 3.10 Pellet samples ready for characterization after sintering process.....	30
Figure 3.11 Calcination profile of ashes product.....	31
Figure 3.12 Sintering profile of the pellet samples.....	31
Figure 3.13 Schematic diagram of a diffractometer system	34

Figure 3.14 XRD Machine.....	34
Figure 3.15 Basic components of an SEM.....	35
Figure 3.16 Scanning Electron Microscope (SEM).....	36
Figure 3.17 Four-Point Probe	37
Figure 3.18 Sample holder set up for resistivity measurement.....	37
Figure 4.1 XRD patterns of ashes sample before calcination.....	38
Figure 4.2 XRD pattern of powder sample after calcination	40
Figure 4.3 Refined XRD pattern of sample without black phosphorus (x=0% wt).....	41
Figure 4.4 Intensity differences patterns for various composition of black phosphorus nanoparticles added $YBa_2Cu_3O_{7-\delta}$ samples.	42
Figure 4.5 SEM image of the sample with x=0.0%	43
Figure 4.6 SEM image of sample with x=2.0%	44
Figure 4.7 SEM image of sample with x=4.0%	44
Figure 4.8 SEM image with sample with x=6.0%	45
Figure 4.9 SEM image with sample with x=8.0%	46
Figure 4.10 SEM image with sample with x=10.0%	46
Figure 4.11 Temperature dependence Resistivity of un-Added and Black Phosphorus added $YBa_2Cu_3O_{7-\delta}$ samples.	47
Figure 4.12 Critical Temperatures of un-added Black Phosphorus added $YBa_2Cu_3O_{7-\delta}$ samples.....	48

LIST OF SYMBOLS AND ABBREVIATIONS

J_c	-	current density
T_c	-	critical temperature
XRD	-	X-ray diffraction
SEM	-	Scanning electron microscope
K	-	Kelvin
E_g	-	minimum energy
k_B	-	Boltzmann's constant
B_c	-	critical magnetic field
B_{c1}	-	lower critical magnetic field
B_{c2}	-	upper critical magnetic field
E	-	electric field
m	-	mass
n_s	-	number density
e	-	charges of electrons
A	-	vector potential
μ_0	-	permeability of the vacuum
λ_L	-	London penetration
F_s	-	free energy density
ξ	-	coherence length
h	-	Planck constants
F_L	-	Lorentz force
F_p	-	pinning force density
N_p	-	number of density of pinning centre
f_p	-	elementary pinning force
d	-	spacing between diffracting planes

- θ - incident angle
- λ - beam wavelength



CHAPTER 1

INTRODUCTION

This chapter provide background of study, problem statement, objectives, scope and significant of study and organization of the report.

1.1 Background of Study

Superconductor is discovered by famous Dutch scientist, Kamerlingh-Onnes soon after he found how to liquefy helium in the early 1900s. He began research into the electrical resistance of very pure metals at cryogenic temperatures. Kamerlingh-Onnes was testing electrical resistance of pure mercury at low temperature in 1911. He found out below 4K, the resistance of mercury decreased to zero. He discovered that mercury enter a new condition below 4K which is called the “superconductivity”. Superconductors are metals, ceramics, and organic materials. Superconductivity occurs when an electrical current is passed through a material that has no resistance. This indicates that superconductor can carry electrons without releasing heat or generating energy. When a superconductor is subjected to a magnetic field, its magnetic lines are expelled out. This effect is known as Meissner effect. High- temperature superconductor was characterized by their complex chemical reaction. Yttrium Barium Copper Oxide (YBCO) is a most widely superconductor that displays high-temperature superconductivity. In 1986, J.G. Bednorz and K.A. Mueller found high-temperature superconductivity in $LaBaCuO_x$ and were given the Nobel Prize in Physics shortly after. This material exhibited a critical temperature, T_c of 35 K. The groups of M.K. Wu and C.W. Chu discovered superconductivity in the $Y - Ba - Cu - O$ system a year later with $YBa_2Cu_3O_{7-\delta}$ also known as “YBCO-123” having a T_c onset of 92 K.

$YBa_2Cu_3O_{7-\delta}$ is the first material discovered to become superconducting above the boiling point of liquid nitrogen (77K).

There are two type of superconductor. Type I superconductors and Type II superconductors are two different types of superconductors. The majority of Type I superconductors are pure metals with conductivity at normal temperature. Type I superconductors were the first to be found and they require a lower temperature to conduct. Type I superconductors include aluminium, mercury, and lead. They were referred to as "soft superconductors." Metal alloys or complicated oxide ceramics are commonly used in Type II superconductors. Type II superconductors commonly known as high-temperature superconductors (HTS) and "hard superconductors". Type II superconductors include YBCO, BSCCO, TBCCO, and HBCCO.

The Yttrium barium copper oxide (YBCO) superconductor is now being studied because of its ease of synthesis, reliability, and low cost. The $YBa_2Cu_3O_{7-\delta}$ superconductor is highly recommended due to its diverse applications. As a consequence, the research for new type of superconductor has never ended since the discovery of superconductivity in $YBa_2Cu_3O_{7-\delta}$ at 92 K.

1.2 Problem Statement

$YBa_2Cu_3O_{7-\delta}$ superconductor is an attractive material for potential applications such as energy storage systems, current limiters, magnetic bearings and so forth due to their comparatively high critical temperature. These applications required a high critical density even with high applied magnetic field. For maintaining high superconducting properties in $YBa_2Cu_3O_{7-\delta}$, it has important limiting factors such as low grain boundary, weak links and poor flux pinning. In the presence of magnetic field, the $YBa_2Cu_3O_{7-\delta}$ results in low current density, J_c and critical temperature, T_c . Current density can be enhanced by preventing the vortex from moving which can be accomplished by pinning flux lines using suitable

impurities which is known as pinning centres materials. Pinning centre materials can be generated by chemical doping or addition of nanoparticles in $YBa_2Cu_3O_{7-\delta}$ superconductor.

Addition of nanoparticles is most currently in research due to its easy process. Nanoparticles such as $BaZrO_3$, ZrO_2 , ZnO , SnO_2 and Al_2O_3 can react with superconductor materials like $YBa_2Cu_3O_{7-\delta}$ and some of them have been shown to have a considerable effect on superconductor critical parameters, notably increasing J_c . The addition of nanoparticles to $YBa_2Cu_3O_{7-\delta}$ system enhance current carrying capability which prevent magnetic flux mobility therefore prevent J_c suppression. Furthermore, the addition of nanoparticles to $YBa_2Cu_3O_{7-\delta}$ system improve current carrying capability due to size of nanoparticles is almost identical to magnetic flux diameter of superconductor. Thus, the addition of nanoparticles is likely to change other superconducting properties of $YBa_2Cu_3O_{7-\delta}$ by locally altering the crystalline structure and generating defects such as twin, tweed, and inhomogeneous micro-defects. In this study, black phosphorus nanoparticles was selected to be pinning centre material in $YBa_2Cu_3O_{7-\delta}$.

Black phosphorus act as pinning centre material is still rare, less study and research was conducted. Since then, black phosphorus was the most stable allotrope of the phosphorus element. Black phosphorene is one of the rare 2D materials having exceptional mechanical, electrical, and optical characteristics for device applications. Black phosphorus has been gaining popularity ever since the fabrication of field-effect transistors. Recent research indicates that 2D Black Phosphorus and its bulk phase have a high charge carrier mobility, in-plane anisotropic structure, and a tunable direct bandgap. Moreover, according to its wider layer spacing and folded structure, 2D Black Phosphorus has a theoretical specific capacity that is 432.8 mAh g^{-1} , which is significantly higher than graphite (372 mAh g^{-1}). Due to the armchair phosphorene nanoribbon structure in Black Phosphorus, it have excellent energy storage capability in both theoretically and experimentally. Therefore, Black phosphorus has emerged as a potential pinning centre material for superconductors.

There are several methods used to synthesized $YBa_2Cu_3O_{7-\delta}$ such as coprecipitation, combustion method and solid-state reaction. Coprecipitation is method

where metal oxalate, carbonate or hydroxide precipitates with cation mole ratio of Y: Ba: Cu = 1: 2: 3 were formed from aqueous solution of metal nitrates. The resulting precursors are acquired in the form of fine powder using this procedure. The difficulty in controls the final composition of the precipitates is an issue in this procedure. The citrate-nitrate auto-combustion reaction was also used to make superconductor ceramic material results in nanostructured homogenous materials with high yield. Solid state reaction was the most extensively used method which allows common compounds to be calcined into superconducting materials. This method has been used to fabricate all the superconductors described in the present work. In 2009, A.Aliabadi used solid state reaction at 840°C for 12 hours to synthesize superconductor $\text{Y}_3\text{Ba}_5\text{Cu}_8\text{O}_{18-\delta}$ (Y38), the last member of YBCO family. With the exception of CuO chains and CuO_2 planes, the sample had T_c around 102 K and crystalline structure of this phase is remarkably similar to $\text{YBa}_2\text{Cu}_3\text{O}_{7-\delta}$. In this study, sample with different composition of Black Phosphorus added into $\text{YBa}_2\text{Cu}_3\text{O}_{7-\delta}$ will prepared using solid state method. Then, the structural and superconductivity properties of sample will be investigated and discussed in this study.

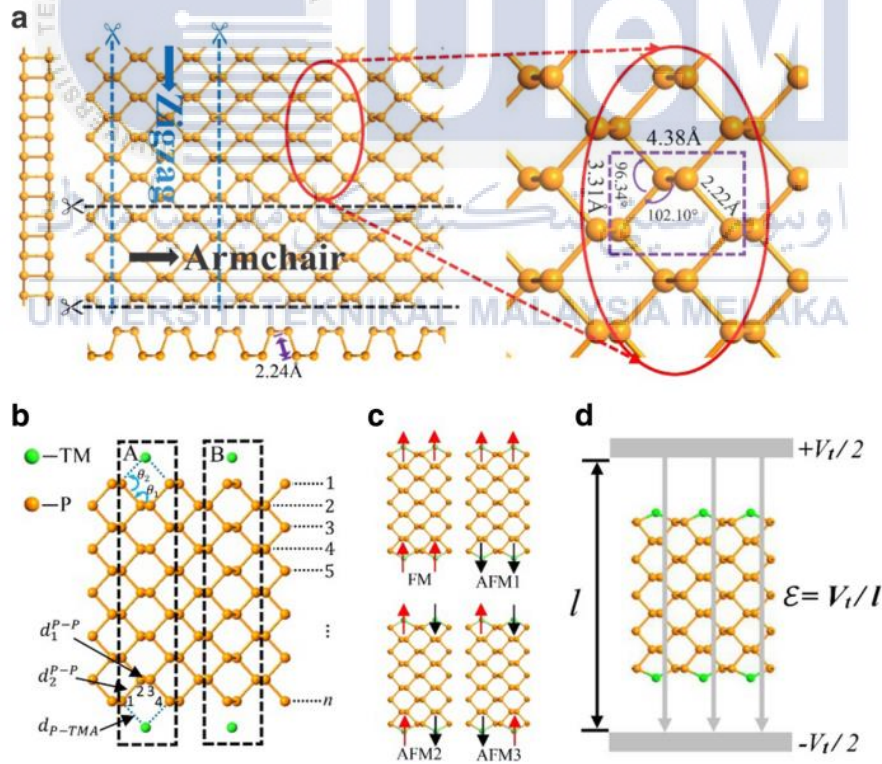


Figure 1.1 Armchair structure of 2D Black Phosphorus

1.2 Objectives

- I. To formulate the Black Phosphorus added $YBa_2Cu_3O_{7-\delta}$ superconducting nanoparticle by using solid-state reaction.
- II. To elucidate the structural properties of Black Phosphorus added $YBa_2Cu_3O_{7-\delta}$ by using X-ray Diffraction (XRD) and Scanning Electron Microscope (SEM) analysis.
- III. To correlate the structural properties of Black Phosphorus with the electrical conductivity of $YBa_2Cu_3O_{7-\delta}$ superconductor by using cryogenic Four-Point Probe.

1.3 Scope of Work

The scopes of this work are synthesizing and characterizing $YBa_2Cu_3O_{7-\delta}$ added black phosphorus nanoparticles produced by solid-state reaction. This study seeks to systematically study the effect of black phosphorus with different weight percentage added into $YBa_2Cu_3O_{7-\delta}$ superconductor target on structural properties and superconducting properties. This study will entail structural analysis utilizing X-ray diffraction (XRD), Scanning electron microscope (SEM) and Resistance-Temperature ($R - T_c$) measurements in sample for superconducting properties will be measure through Four- Point Probe. To summarize, this study will introduce black phosphorus as pinning centre material to increase the superconducting properties with minimum effects toward T_c of $YBa_2Cu_3O_{7-\delta}$ superconductor.

1.4 Significance of Study

This research presents a method of synthesizing superconductors composite. Black phosphorus nanoparticles were introduced as pinning centre materials and distributed into $YBa_2Cu_3O_{7-\delta}$ superconductor. The black phosphorus shows great potential as a candidate for pinning centre materials and has attracted tremendous interest in the scientific community due to its advantageous structural properties and higher carrier mobility. The method used in this study is solid state reaction which has higher productivity and lower cost. The reaction efficiency in this technique is great and provides better distribution in high temperature superconductor. As a result, the structural and superconducting properties of $YBa_2Cu_3O_{7-\delta}$ are expected to be increased.

1.5 Organization of Report

There are five chapters included in this project. Chapter 1 describes background study, problem statement, objectives, scope of work and significance of study are covered in order to complete this project. Chapter 2 describes about the literature review based on the project. This chapter provides basic theory about superconductors and characteristics of type II superconductor. Chapter 3 describes the details about preparation of sample and characterization techniques used in this project. For chapter 4, which is results and discussion will discuss about the results obtained from this study. Lastly, chapter 5 describes about conclusion of this project and recommendation in this study.

1.6 Summary

This chapter has successfully described the background of this study and a brief introduction of this study.

CHAPTER 2

LITERATURE REVIEW

This chapter is mainly describe the theory and research which have been defined and done by various researcher years ago. Related information of previous studies are extracted as references and discussion based on their research about YBCO superconductor, structure, mechanical and physical properties.

2.1 A Brief History of Superconductivity

Heike Kamerlingh Onnes discovered superconductivity in 1911 while studying the characteristics of metals at low temperatures. He became the first one to liquefy helium which has a boiling point of 4.2 K at atmospheric pressure. This had opened up a new range of temperature for experimental study. During his research on the conductivity of metals at low temperatures, he discovered that just at the boiling temperature of liquid helium the resistance of mercury sample decreased to an unmeasurable low value. Figure 2.1 shows the initial measurement. This unexpected phenomenon was called “superconductivity” by Karmmerlingh Onnes. The critical temperature (T_c) is known as the temperature below which the mercury becomes superconducting.

Over the next 75 years, scientists made significant progress in their understanding of superconductors. During that period, various alloys that were superconductors at slightly higher temperatures were discovered. Unfortunately, none of these alloy superconductors was capable of operating at temperatures higher than 23 K. As a result, liquid helium remained the sole practical refrigerant for use with these superconductors. Many additional

elements have been revealed to be superconductors after this discovery. In 1980, superconductivity had been discovered in numerous metals and alloys. Remarkably, traditional ferromagnets like Nickel (Ni) and Iron (Fe) did not show superconductivity. Superconductivity has only been documented in the non-magnetic state and under very high pressure. For example, in iron, $T_c=2$ K. Discovery of superconductors with high T_c has been a strong motivation since the beginning. However, until 1980 the A-15 compound, Nb_3Ge was the superconductor with highest T_c around 22 K. Thus, many alloys and impact of applying pressure were investigated an attempt to obtain higher T_c values.

Consequently, numerous possible applications were ruled out due to lack of commercial viability. Furthermore, most scientists consider superconductivity as a small field with limited potential for increasing critical temperatures. All this suddenly changed when K. A. Bednorz and J. G. Müller discovered high-temperature superconductivity. New superconductors from different material classes were discovered shortly after 1980. K. A. Bednorz and J. G. Müller published a paper in April 1986 on the possibility of superconductor in ceramic material called La – Ba – Cu – O with T_c around 35K. This was the first cuprate superconductor to be discovered. Müller and Bednorz said that the French work on La – Ba – Cu – O system inspired their research. The era of “High-Temperature Superconductivity” began when the researchers from the University of Tokyo validated Müller and Bednorz findings.

At the end of 1986 and the beginning of 1987, the discovery of Y – Ba – Cu – O (YBCO) superconductor with a T_c of 92 K was highlighted by the synthesis of rare-earth metal oxides with higher T_c . This is a huge breakthrough because the material was become superconducting above 77K, the boiling point of liquid nitrogen. Because of the simplicity in which YBCO could be synthesized, it was investigated by a several laboratories. In February 1988, researchers from Japan, China and the United States discovered superconductivity in copper-containing oxides without rare earth. Bismuth or thallium are included in these non-rare earth superconductors. These superconducting compounds have been reported with T_c around 127 K. In addition, unlike rare earth superconductors, these materials are more stable since they do not lose oxygen or react with water. Figure 2.3 show history of some of the discovered superconducting compounds.

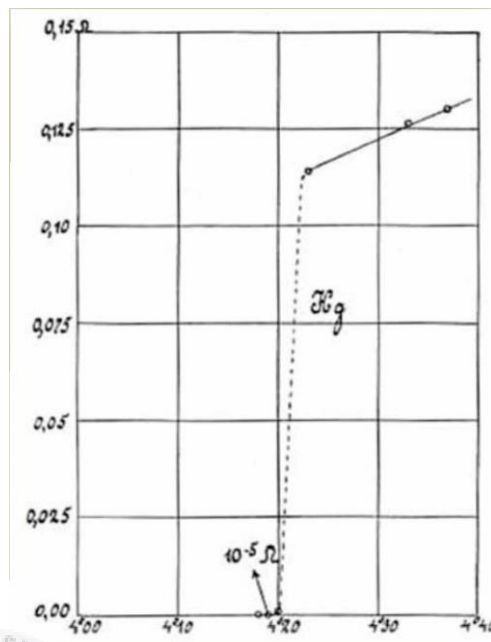


Figure 2.1 Illustration of Kamerlingh Onnes' discovery of superconductivity

Superconductive Elements

At ambient pressure

At high pressure

1 H																	2 He														
3 Li	4 Be																	5 B	6 C	7 N	8 O	9 F	10 Ne								
11 Na	12 Mg																	13 Al	14 Si	15 P	16 S	17 Cl	18 Ar								
19 K	20 Ca	21 Sc	22 Ti	23 V	24 Cr	25 Mn	26 Fe	27 Co	28 Ni	29 Cu	30 Zn	31 Ga	32 Ge	33 As	34 Se	35 Br	36 Kr														
37 Rb	38 Sr	39 Y	40 Zr	41 Nb	42 Mo	43 Tc	44 Ru	45 Rh	46 Pd	47 Ag	48 Cd	49 In	50 Sn	51 Sb	52 Te	53 I	54 Xe														
55 Cs	56 Ba	57 La	72 Hf	73 Ta	74 W	75 Re	76 Os	77 Ir	78 Pt	79 Au	80 Hg	81 Tl	82 Pb	83 Bi	84 Po	85 At	86 Rn														
87 Fr	88 Ra	89 Ac	104 Rf	105 Ha	106 Sg	107 Bh	108 Hs	109 Mt	110 Ds	111 Rg	112 Uub																				
																		58 Ce	59 Pr	60 Nd	61 Pm	62 Sm	63 Eu	64 Gd	65 Tb	66 Dy	67 Ho	68 Er	69 Tm	70 Yb	71 Lu
																		90 Th	91 Pa	92 U	93 Np	94 Pu	95 Am	96 Cm	97 Bk	98 Cr	99 Es	100 Fm	101 Md	102 No	103 Lr

Figure 2.2 Superconductive Elements in Periodic Table

Based on the figure above, elements with red colour were found to be superconducting at ambient pressure whereas elements with blue colour were found to be superconducting under high pressure.

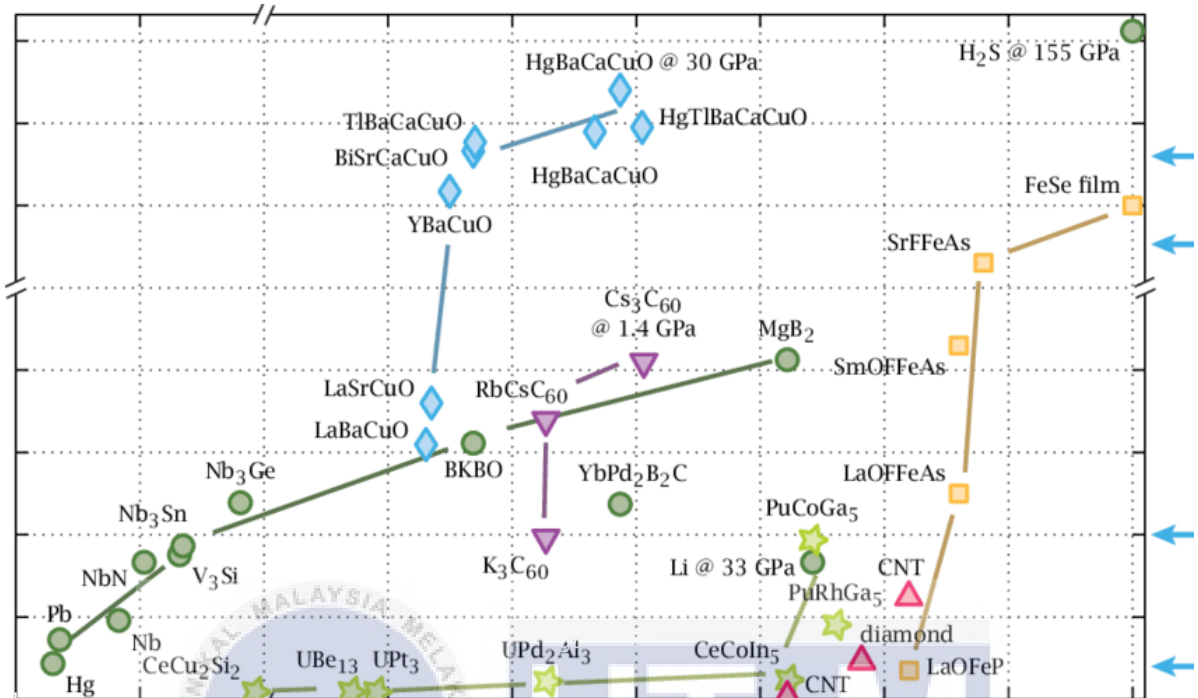


Figure 2.3 History of some of the Superconducting Compounds

2.2 Zero Resistance in Superconductors

In general, all conductors resist current flow. This resistance which is measured in ohms causes energy to be dissipated in the form of heat. These materials transport currents and when they have low resistance only a little amount of energy is consumed which make them extremely efficient. It is commonly understood that metals contain a large number of free electrons and electric current is a flow of these electrons. Electrons are constantly scattered because all metals contain impurities and atoms oscillate. As a result, experiencing zero electrical resistance appears to be impossible. However, in superconductors, there is no electrical resistance. It can be proved that if an electric current is started in a circular superconductor, it will flow endlessly. This is a completely unexplained phenomenon and it is a mystery that many physicists are trying to solve. Therefore, three scientists (Bardeen, Cooper, and Shrieffer) proposed the final answer, which is now known as the BCS theory. J. Bardeen, L.N. Cooper, and J.R. Schrieffer unveiled the underlying microscopic BCS theory of superconductivity in 1957.

BCS theory describes that at low temperatures, electrons can form into pairs which are known as Cooper pairs and flow through superconductors without resistance. This theory states that superconductivity is the result of numerous electron pairs forming and condensing. Cooper proved that in metal, a small attraction between electrons can cause a paired state of electrons to have lower energy which indicates that pair is bound. In conventional superconductors, this attraction is caused by the electro-phonon interaction. This attraction, according to the BCS theory, pulls positive ions closer to the passing electron resulting in a region with a larger positive charge density. This region of higher positive charge density moves with the electron. Because of their "atomic cupid," the crystal lattice, two electrons get indirectly bonded and form a Cooper pair. The production of Cooper pairs and their impact on superconductivity is a complex quantum process that required a comprehensive understanding of quantum mechanics.

The energy gap or known as bandgap in superconductors is defined as the amount of energy need to separate Cooper pairs and create normal electrons. The energy gap also implies phase changes and states that all electrons must be at the same energy level. The measured band gap in superconductors is one of the experimental devices which support the BCS theory. One of the key predictions in this theory was that a minimum energy, E_g should be required to break a pair by the equation:

$$E_g = \frac{7}{2} k_B T_c \quad \text{Equation 2.1}$$

Where is k_B is Boltzmann's constant and T_c is critical temperature.

The condensation of electrons into state that leaves an energy gap above them occurs when a metal transitions from its normal to the superconducting state. Thus, cooper pair is a superfluid that can flow without energy dissipation. As a consequence of this, the resistivity of superconductors is zero. Superconductors are well known to the general public because of their characteristics with zero resistivity and no heat losses for currents flow through them. They could have a variety of application which includes superconducting magnets, superconducting power transmission, and electricity storage.

2.3 Meissner Effect

Superconductors have two significant properties, they conduct electric current with zero resistance and expel magnetic field. When a magnetic field is applied to a typical metal, the magnetic field will penetrate the metal. The expulsion of a magnetic field is called the Meissner effect. The expulsion of a magnetic field from the interior of material is in the process of becoming superconducting and losing its resistance to the flow of electric currents when cooled below a specific temperature, usually near to absolute zero. It can be said that this phenomenon is different from perfect conductivity. In 1933, German physicists W. Meissner and R. Ochsenfeld discovered the Meissner effect which is a property of all superconductors. The Meissner effect is a major characteristic of superconductivity and it helps to distinguish superconductivity from the absence of electrical resistance.

It is also worth mentioning that superconductors are categorized into two groups. Type I and type II superconductors have extremely distinct magnetic characteristics. There is only one magnetic critical field B_c in type I superconductors. Type I superconductors completely expel an applied magnetic field. The most common type I superconductors are Lead (Pb), Mercury (Hg), Niobium (Nb) and Tin (Sn). The magnetic flux of a superconductor can expel when magnetic field applied to a superconductor is larger than the magnetic critical field B_c . As a result superconducting state is destroyed. When magnetic flux enters a superconducting sample, it returned to its normal condition. Meissner currents occur when magnetic fields are below a certain magnetic critical field B_c therefore prevents penetration of magnetic field into the sample. Figure 2.4 shows the schematic diagram for type I superconductor of magnetic field versus temperature.

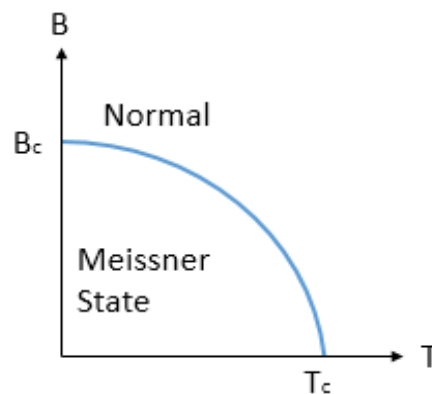


Figure 2.4 Schematic B-T phase diagram for Type I superconductors

For type II superconductors, there is an extra state that occurs between Meissner State and the normal state. This state is a mixture of normal and Meissner state, also known as the mixed state or Vortex state. The magnetic field is allowed to flow through the superconductor where the normal state is present, whereas the rest of superconductors shows the Meissner effect and expels magnetic field. B_{c1} and B_{c2} are the critical magnetic fields in these superconductors. B_{c1} represents the lower critical magnetic field while B_{c2} represents the upper critical magnetic field. The quantized magnetic fluxes will penetrate in these superconductors when the magnetic field satisfies $B_{c1} < B < B_{c2}$, which generates an Abrikosov lattice also known as flux lines or flux tubes. Each flux line carries a quantum of magnetic flux. Figure 2.5 shows the schematic B-T phase diagram for a type II superconductor.

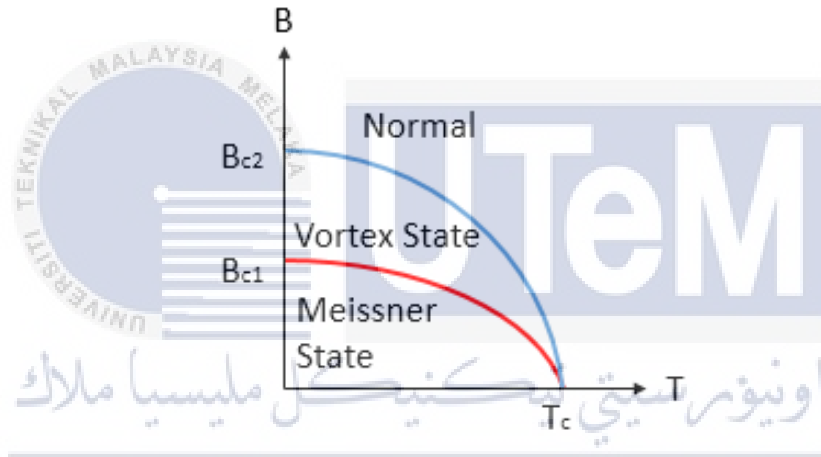


Figure 2.5 Schematic B-T phase diagram for Type II superconductors

2.4 Theory of Superconductivity

2.4.1 London Theory

In 1935, the London brothers proposed a simple but efficient theory of the electrodynamics of superconductivity shortly after the discovery of magnetic fields are expelled from superconductors. The development of a pair of equations relating the electric field, E and the magnetic field, B to the current density, j

$$E = \frac{\partial(\Delta j)}{\partial t} \quad \text{Equation 2.2}$$

$$B = -\nabla \times (\Delta j) \quad \text{Equation 2.3}$$

Where $\Delta = \frac{m}{n_s e^2}$ is a phenomenological parameter linked to m , is the mass of an electron, n_s is the phenomenological constant associated with the number density of superconducting and e is the charges of electrons.

The London brothers were able to theoretically define the Meissner effect by assuming that the current density, j in a superconducting state is directly proportional to the specific vector potential, A of the magnetic field, B where :

$$B = \nabla \times A \quad \text{Equation 2.4}$$

Then, these two equations can be combined into a single “London Equation”

$$\nabla \times j = -\frac{n_s e^2}{m} B \quad \text{Equation 2.5}$$

In the term of specific vector potential A , giving

$$j = -\frac{n_s e^2}{m} A \quad \text{Equation 2.6}$$

Under static conditions, one of the Maxwell equations reduced to

$$\nabla \times B = u_0 j \quad \text{Equation 2.7}$$

Where u_0 is the permeability of the vacuum.

Then, by substituting this equation for j into equation 2.3, can obtain

$$B = -\frac{\Delta}{u_0} \nabla \times (\nabla \times B)$$

$$B = \frac{\Delta}{u_0} \nabla^2 B$$

$$B = \frac{m}{u_0 n_s e^2} \nabla^2 B \quad \text{Equation 2.8}$$

It can be written as,

$$\nabla^2 B = \frac{1}{\lambda_L^2} B \quad \text{Equation 2.9}$$

Where $\lambda_L = \sqrt{\frac{m}{u_0 n_s e^2}}$ is the characteristic length scale which is known as “London penetration depth”. This equation also can be written as

$$B(x) = B_0 e^{-x/\lambda} \quad \text{Equation 3.0}$$

2.4.2 Ginzburg-Landau Theory

Ginzburg-Landau theory also known as Landau-Ginzburg theory is a mathematical physical theory that describes superconductivity. It is name after Vitaly Ginzburg and Lev Landau. The Ginzburg-Landau Theory is a phenomenological explanation of superconductivity in terms of thermodynamics. It is paramount importance in the history of superconductivity. This theory starts from the deduction of the Landau free energy density. Ginzburg and Landau assumed that free energy density, F_s can be expressed as a function with complex order parameters. The equation can be written as:

$$F_s = F_n + \alpha |\phi|^2 + \frac{\beta}{2} |\phi|^4 + \frac{1}{2m} (-i\hbar\nabla - 2eA)\phi|^2 + \frac{B^2}{2\mu_0} \quad \text{Equation 3.1}$$

Where F_n is the free energy in normal phase, α and β are phenomenological constants, m is effective mass, e is charge of an electron, A is the magnetic potential vector and \hbar is the Planck constants.

By minimizing the equation to ϕ as:

$$\alpha \phi + \beta |\phi|^2 + \frac{1}{2m} (-i\hbar\nabla - 2eA)\phi|^2 = 0 \quad \text{Equation 3.2}$$

To determine the equation for current density J , take the derivative of F_s , to magnetic potential A , gives the second Ginzburg-Landau equation:

$$J = \frac{e}{m} [\psi^* (-i\hbar \nabla - 2eA) \psi] \quad \text{Equation 3.3}$$

This theory introduced coherence length which explained the size of thermodynamic fluctuations during superconducting phase:

$$\xi = \sqrt{\frac{\hbar^2}{4m\alpha(T)}} , \text{ when } T < T_c \quad \text{Equation 3.4}$$

$$\xi = \sqrt{\frac{\hbar^2}{2m\alpha(T)}} , \text{ when } T > T_c \quad \text{Equation 3.5}$$

2.5 Flux Pinning in Type II Superconductors

Type II superconductors can deliver high currents in a strong magnetic field. In type II superconductors, the vortices can flow without restrictions which cause motion of vortices and energy dissipation. When type II superconductor is in the mixed state the transport current is zero. It is necessary for these superconductors to have capability in carrying large critical currents in order to achieve the practical use of type II superconductors. Large critical currents lead to Lorentz forces. Thus, pinning force was used to repel Lorentz forces and can prevent movement of vortices. The equation of Lorentz force as:

$$F_L = J \times B \quad \text{Equation 3.6}$$

Where J is critical currents density and B is the magnetic field.

Flux lines have spatial structures related to order parameters, ϕ and magnetic field, β . When the flux line is near the pinning centre, variation in the energy occurs due to overlapping of these structures with a special structure of pinning centre. This phenomenon is known as pinning interaction where the flux lines suffered a pinning force. The pinning force density will stop the flux line lattice from opposing the Lorentz force. The resultant pinning force density, F_p is related with the number of density of pinning centre material N_p with the relations as follows:

$$F_p = N_p f_p \quad \text{Equation 3.7}$$

Where f_p is elementary pinning force which is defined as the maximum pinning strength of an individual pinning centre.

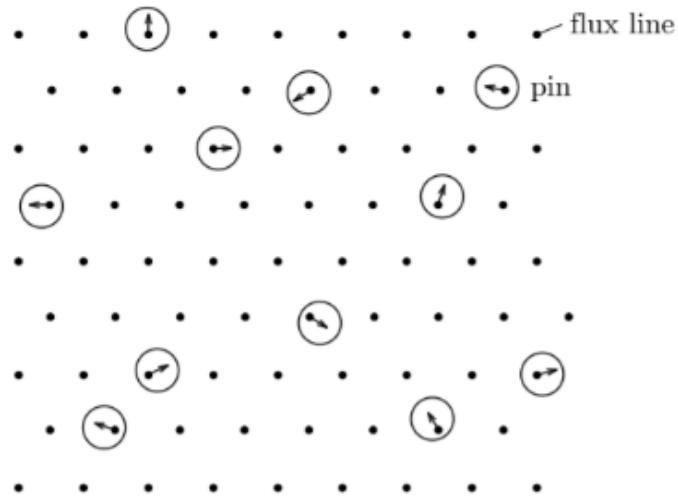


Figure 2.6 Forces of pinning centre distributed randomly

2.6 YBCO Superconductor

Among superconductors, low-temperature superconductors (LTS) have a critical temperature below 30K while the high-temperature superconductors (HTS) have a critical temperature above 30K. Many high-temperature superconductors have been discovered over the last 30 years. Due to their electrical and magnetic characteristics, there is a huge interest in these materials throughout the world. In 1986, Georg Bednorz and Alex Muller discovered superconductivity above 30K in the $La - Ba - Cu - O$ system. As a result, the superconducting phase as $La_{2-x}Ba_xCuO_4$ is identified. Some of researchers were then begun to determine the effects of elemental substitutions, various processing conditions on the structure and superconducting features of this oxide. By using this approach, Paul Chu, Maw-Kuen Wu, and coworkers discovered superconductivity above 90K in the $Y - Ba - Cu - O$ system in 1987.

YBCO is one of the most important copper oxide-based superconductors and it has gained a lot of attention since Wu(1987) first announced it. YBCO was the first superconductor found with $T_c > 77K$. In recent years, research has been focused on methods of producing and determining the physicochemical properties of $YBa_2Cu_3O_{7-\delta}$ (YBCO).

Because of its stoichiometric composition, the $YBa_2Cu_3O_{7-\delta}$ compound is generally known as $Y-123$. It is one of the most significant and popular superconducting materials. $YBa_2Cu_3O_{7-\delta}$ provide numerous advantages which included a high J_c , a high T_c , superior magnetic field trapping capabilities and excellent mechanical characteristics.

The crystal structure of $YBa_2Cu_3O_{7-\delta}$ superconductor is shown in figure 2.5. The Cu is located in the corner of a unit cell and it has two distinct coordinates with oxygen which is $Cu(1)$ and $Cu(2)$. $Cu(1)$ between two barium planes created one dimensional $Cu(1) - O(1)$ chain in the orthorhombic phase. The other site labelled $Cu(2)$ between Y and Ba planes generated two-dimensional $Cu(2) - O(2,3)$ planes in the orthorhombic phase. The perovskite structure has 9 oxygen atoms whereas the $YBa_2Cu_3O_{7-\delta}$ has 7 oxygen atoms which is also known as an oxygen-deficient multi-layer perovskite structure. The formula $Y_1Ba_{3-1}Cu_3O_9$ is obtained by tripling the perovskite (ABO_3) unit cell and substituting one yttrium atom for every third barium tom. On the other hand, superconductivity required a little more than two oxygen vacancies. Thus, $Y_1Ba_{3-1}Cu_3O_{9-x}$ can be thought of as the formula. The unit cell is orthorhombic which consists of nearly three cubes stacked on top of each other.

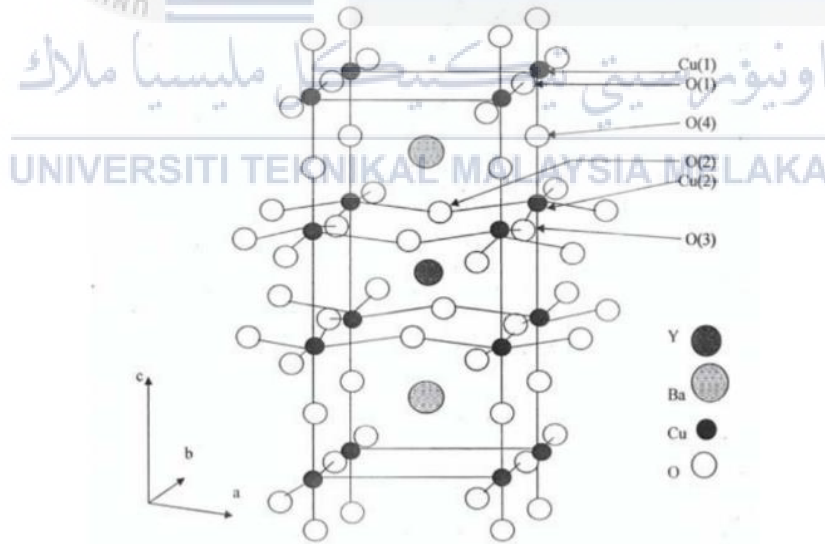


Figure 2.7 Structure of $YBa_2Cu_3O_{7-\delta}$ superconductor

2.7 Addition of Nanoparticles in $YBa_2Cu_3O_{7-\delta}$

The findings for a new type of superconductor has never ended since the discovery of superconductivity in $YBa_2Cu_3O_{7-\delta}$ at 92K. $YBa_2Cu_3O_{7-\delta}$ superconductor is granular

therefore it contributes to inhomogeneity in bulk samples, weak grain boundary connections and poor flux pinning. As a consequence, in the presence of a magnetic field, T_c and J_c are low. According to research, nanostructure materials and carbon-based compounds can be used in high temperature superconductors to produce high J_c at high magnetic fields. The addition of rare earth nanoparticles to the $YBa_2Cu_3O_{7-\delta}$ system improved its current carrying capabilities since the size of nanoparticles remarkably similar to magnetic flux diameter of a high-temperature superconductor. The nanoparticles may act as pinning centres to prevent movement of magnetic flux thus increasing J_c .

It is well known that artificial pinning centres have been effectively introduced into superconductor by the addition or substitution of elements such as micro and nanoparticles, magnetic and non-magnetic materials and numerous compounds. Many research projects were launched by various academic researchers but the addition of the most appropriate nanosized material is still chosen for the enhancement of superconducting properties. It was found that adding ZrO_2 and ZnO nanoparticles to $GdBa_2Cu_3O_7$ superconductor improved superconducting parameters. In polycrystalline $YBa_2Cu_3O_{7-\delta}$ superconductor, the inclusion of $ZnMnO$ nanoparticles has enhanced strength of flux pinning. It was observed that the addition of nano- Al_2O_3 particles to superconductors dramatically increased J_c in the applied magnetic field which attributed to the existence of improved flux pinning centres. The addition of nano- Al_2O_3 particles to polycrystalline $(Bi,Pb) - 2223$ superconductor enhanced the values of pinning force density, onset temperature, activation energy and J_c . From the research finding, the bulk superconductor $YBa_2Cu_3O_{7-\delta}$ was doped with Ag nanoparticles of various sizes and different concentrations which results in a monotonic improvement in superconducting parameters particularly increase J_c , leading to better crystallite connectivity and superconducting volume fraction. To be used as dopants, the nanoparticles must comply with the following requirements. Their presence should not influence on the formation of superconducting phase. Also, they should not aggregate together and maintain their nanosize character.

Presently, the perovskites-based titanate $BaTiO_3$ is currently an important material for a variety of applications because of its mechanical, chemical and thermal durability. In general, $BaTiO_3$ nanoparticles functioned as one-dimensional artificial pinning centres for their scale of coherence length of $YBa_2Cu_3O_{7-\delta}$. The homogeneous dispersion of $BaTiO_3$

nanoparticles within the $YBa_2Cu_3O_{7-\delta}$ matrix created a unique microstructure that allowed flux pinning to be strengthened. It has been published that combining this material with other types of nanoparticles has been suggested as a way to improve $YBa_2Cu_3O_{7-\delta}$ superconducting properties. In contrast, tungsten oxide, WO_3 has been widely used in a variety of technical applications in recent years due to its physicochemical features, redox potential, higher melting point, excellent photocatalytic properties and excellent strength. The observational results revealed that addition of WO_3 nanoparticles into $YBa_2Cu_3O_{7-\delta}$ are effective in improved flux pinning ability and enhanced superconducting properties of $YBa_2Cu_3O_{7-\delta}$.

In summary, the addition of nanoparticles into YBCO system strengthened the current- carrying capability which prevented magnetic flux mobility and hence prevented current density suppression. However, the addition of nanosize particles is likely to alter other superconducting properties of $YBa_2Cu_3O_{7-\delta}$ such as T_c by locally changing the crystalline structure, forming defects such as twins, tweed and inhomogeneous micro-defects. As a consequence, it is important to increase the critical current density of $YBa_2Cu_3O_{7-\delta}$ bulk superconductor in an effort to promote practical applications. The number of effective pinning centres should be increased in order to improve performance of $YBa_2Cu_3O_{7-\delta}$ superconductors.

UNIVERSITI TEKNIKAL MALAYSIA MELAKA

2.8 Black Phosphorus

Phosphorus which belongs to the 15th group of periodic table, is the most plentiful element is earth. Phosphorus has been investigated as a key element in plants and animals for nearly 300 years. White, red and black phosphorus are the three most prevalent allotropes. Phosphorus has developed enormously as an inorganic nanomaterial in the era of nanotechnology. Nanomaterials have a configurable bandgap, quantum confinement effect, good light absorption capabilities and high carrier mobility.

In 1914, Bridgman produced black phosphorus (BP) for the first time at 200°C under high pressure. In a high pressure cylinder with kerosene, white phosphorus was placed. High pressure of 0.6 GPa was used at room temperature. The pressure was then increased to 1.2 GPa and the cylinder temperature was raised to 200°C. Under these conditions, it took 5 to 30 minutes to change white phosphorus to black phosphorus. A small amount of black phosphorus was found after cylinder is cooled and released the pressure. Bridgman discovered that black phosphorus has a high density of 2.69gcm^3 compared to 1.83gcm^3 for white phosphorus and around $2.05 - 2.34\text{gcm}^3$ for red phosphorus. Unlike the previously mentioned procedures of synthesis using white phosphorus, researchers later began using red phosphorus as a raw material for generating BP to prevent toxicity in white phosphorus. In 2007, Lange et al. discovered that BP could be made from red phosphorus by adding a modest amount of gold, nickel and nickel(IV)iodide at 600°C in low pressure conditions. Later in year 2014, Kopf et al. proposed that BP may be made using red phosphorus, tin and tin(IV)iodide additives using a short-way transport reaction. Moreover, unlike white phosphorus and red phosphorus, BP conclusively showed chemical stability and it could withstand high temperature of 400°C without spontaneous ignition.

Black Phosphorus is one of the most stable allotropes of phosphorus. It has been evaluated as an essential layered material recently after 2014. The two-dimensional (2D) black phosphorus shows extensively advantages compared to well-studied 2D nanomaterials such as graphene and transition metal dichalcogenides (TMDs). Graphene has remained one of the most researched materials since its discovery in 2004 and has remarkable electrical and physical properties. However, it is limited by absence of a bandgap which limits being used in the semiconductor field. As a result, a lot of effort went into finding alternative 2D semiconductors which include black phosphorus. BP shows as an excellent conductor of electrons although less diamagnetic than white and red phosphorus. The Brigman method has also been shown to transform the solid structure of BP from amorphous to polycrystalline form based on the applied pressure and temperature. Keyes and Warschauer both reported on the electrical and optical characteristics of polycrystalline BP. According to their findings, polycrystalline BP is a p-type semiconductor with a room temperature of approximately 1Ω and energy gap of around 0.35eV .

2.9 Solid-State Reaction

A solid-state reaction is a typical synthesis method for obtaining polycrystalline material from solid reagents. A very high temperature is generally used for the reaction to occur. The factors that affect solid-state reaction are chemical and morphological features of the reagents such as resistivity, surface area and free energy change with solid-state reaction. Others reactions parameters such as temperature, pressure and the reaction environment also affect solid-state reactions. The advantages of this reaction are simplicity and large-scale production. In recent years, research on solid-state reactions at ambient and near ambient temperatures has made a significant process. The use of a solid-state reaction to produce nanomaterials is a new technology that has been established recently. The requirement for nanocrystalline preparation is a clean surface, controllable particle shape, simple collection, and high stability. The solid-state reaction is straightforward can be used with benefits such as easy synthesis, high yield, high selectivity and reduced pollution. Research has proved that solid-state reaction can used to synthesis $YBa_2Cu_3O_{7-\delta}$ superconductor. For instance, synthesis and effect of Al_2O_3 added in $YBa_2Cu_3O_{7-\delta}$ by solid state reaction, effect of Ni_2O_3 addition of $YBa_2Cu_3O_{7-\delta}$ superconductor via solid-state reaction, microstructure and normal state properties for $YBa_2Cu_3O_{7-\delta}$ system added by $ZnFeO$ using solid-state reaction.

CHAPTER 3

METHODOLOGY

In this chapter, details of sample preparation and characterization techniques are presented. Preparation of samples is divided into two parts. The first part is preparation of $YBa_2Cu_3O_{7-\delta}$ samples and the second part is synthesizing different compositions of Black Phosphorus added into $YBa_2Cu_3O_{7-\delta}$ samples. In Section 3.1, all materials used for preparing the samples are introduced. The relevant parameters used in synthesizing the sample is briefly explained in Section 3.2. In Section 3, structural and mechanical characterization techniques and tools of the samples is specified.

3.1 Materials

The materials used for samples preparation are Yttrium Nitrate Hydrate ($Y(NO_3)_3 \cdot 6H_2O$), Barium Nitrate ($Ba(NO_3)_2$), Copper Nitrate Hydrate ($Cu(NO_3)_2 \cdot 3H_2O$), Citric Acid ($C_6H_8O_7$), and Ammonia Hydroxide (NH_4OH). The details of raw materials used to prepare stock solutions are summarized in Table 3.1.

Table 3.1 Raw materials used to prepare stock Solutions

Material	Manufacturing Company	Molecular weight (g/mol)	Concentration (M)
$Y(NO_3)_3 \cdot 6H_2O$	ALFA AESAR	383.01	0.50
$Ba(NO_3)_2$	QREC (ASIA) SDN BHD	261.34	0.25
$Cu(NO_3)_2 \cdot 3H_2O$	QREC (ASIA) SDN BHD	241.60	0.50
$C_6H_8O_7$	GREEN SCIENTIFIC ENTERPRISE	192.124	0.50
NH_4OH	MERCK KGAA	35.05	1.00

3.2 Samples Preparation

3.2.1 $YBa_2Cu_3O_{7-\delta}$ Samples Preparation

First, the $Y(NO_3)_3 \cdot 6H_2O$, $Ba(NO_3)_2$ and $Cu(NO_3)_2 \cdot 3H_2O$ were weighed and transferred to beaker containing distilled water. The weight of material was calculated using Equation 3.1.

$$\frac{\text{moles}}{l} \times 0.025l \times \frac{\text{weight}}{\text{mole}} = \text{amount to weigh out} \quad \text{Equation 3.8}$$

Table 3.2 Amount of Materials

Materials	Concentration, M (<i>moles/ l</i>)	Mass (g)
$Y(NO_3)_3 \cdot 6H_2O$	0.50	4.787
$Ba(NO_3)_2$	0.25	1.633
$Cu(NO_3)_2 \cdot 3H_2O$	0.50	3.020
$C_6H_8O_7$	0.50	2.882

Place this beaker on magnetic stirrer and stirred the solution with moderate stirring speed. Then, the Y, Ba, and Cu nitrate stock solutions were mixed at mole ratio of 1:4:3. Citric acid with concentration of 0.5M was added to the mixture solution which is subjected to the c/n ratio 0.7.



Figure 3.1 $Y(NO_3)_3 \cdot 6H_2O$

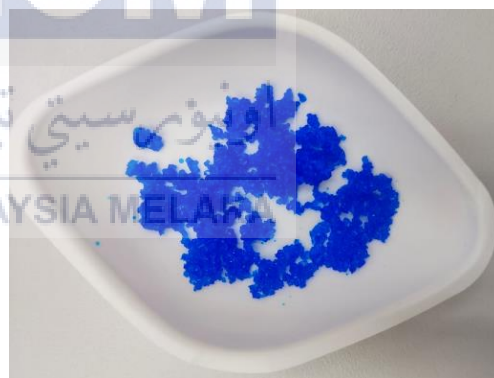


Figure 3.3 $Cu(NO_3)_2 \cdot 3H_2O$



Figure 3.2 $Ba(NO_3)_2$



Figure 3.4 $C_6H_8O_7$



Figure 3.5 Mixture Solution Placed on Hot Plate

3.2.2 Auto- Combustion of the Gel

While all powder dissolved, the mixture solution turned clear blue. The PH value of mixture solution was adjusted to 7 by the addition of ammonia solution. The mixture solution was heated to 250°C on hot plate under infra-red radiation to achieve uniform heating. This process transformed the solution into gel as shown in Figure 3.6. The gel spontaneously combusted by continuous heating to form fine ashes which is brownish-black in colour. The physical changes of the mixture solution through auto-combustion process are depicted in Figures below.

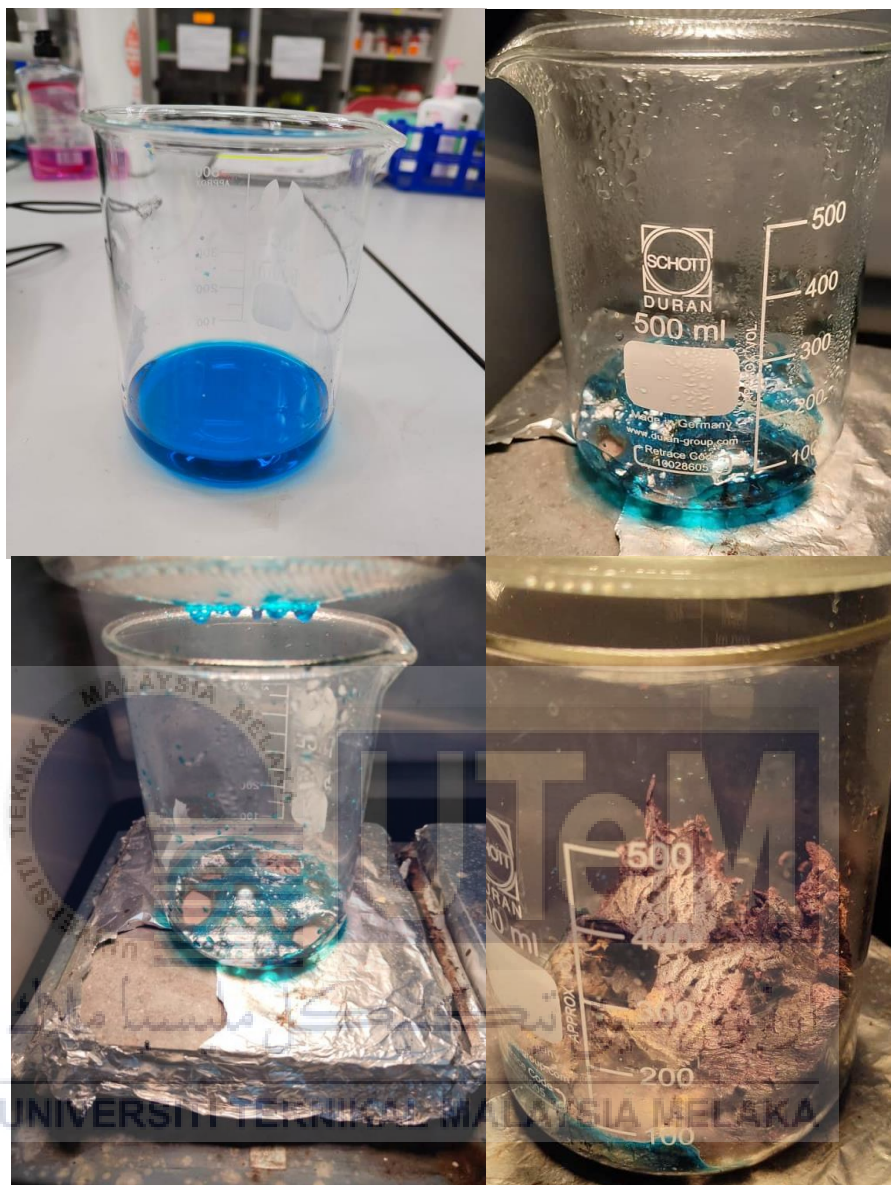


Figure 3.6 Physical Appearance of Samples; (a) Mixture Solution, (b) Solution turned Gel, (c) Flammable Combustion, (d) Fine Ashes Product

3.2.3 Calcination Process

When the entirety of the solution is consumed, turn off the heating knob. The obtained fine ashes product was collected in alumina boat using spatula. The ashes were calcined in furnace at 900°C for 1 hour soaking time under normal atmosphere to yield stable black powder.



Figure 3.7 Resultant Powders Before Calcination

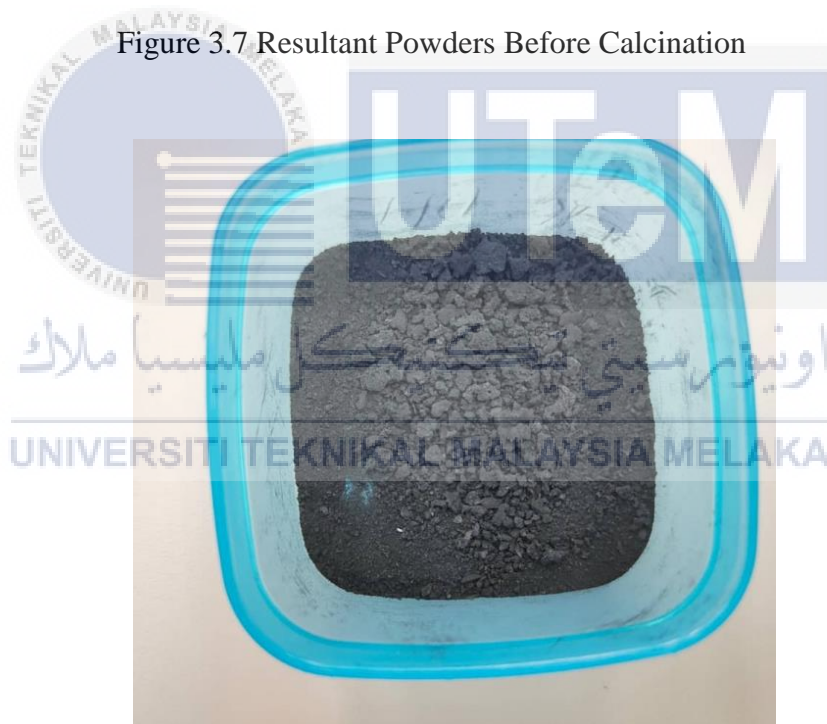


Figure 3.8 Resultant Powders After Calcination

3.2.4 Black Phosphorus Added $YBa_2Cu_3O_{7-\delta}$ Samples

After calcination process, Black Phosphorus was added into $YBa_2Cu_3O_{7-\delta}$ powder. The additional amount, x wt. % of Black Phosphorus in this case varied from 0.0 wt. % to 10.0 wt. % of the total mass of the sample. Next, ground the powder in a mortar and pestle to obtain fine particles. The as-prepared powder sample was pressed in the form of cylinder-shaped pellets of 0.4 g each.

Table 3.3 Amount of Black Phosphorus added into $YBa_2Cu_3O_{7-\delta}$

Sample	$YBa_2Cu_3O_{7-\delta}$ Powder	wt. % of Black Phosphorus	Amount of Black Phosphorus (g)
1	0.4	0.0	0.000
2	0.4	2.0	0.008
3	0.4	4.0	0.016
4	0.4	6.0	0.024
5	0.4	8.0	0.032
6	0.4	10.0	0.040

3.2.5 Sintering Process

The calcined powder was pelletized into disk by applying 5 tons. Pellet samples were sintered at 900°C for 1 hour under normal atmosphere in furnace using alumina boat. Each pellet was self-cooled to room temperature. The pellets which were ready for characterization is shown in Figure 3.9. The calcination and sintering profile are depicted in Figure 3.11 and 3.12



Figure 3.9 Pelletized Machine



Figure 3.10 Pellet samples ready for characterization after sintering process

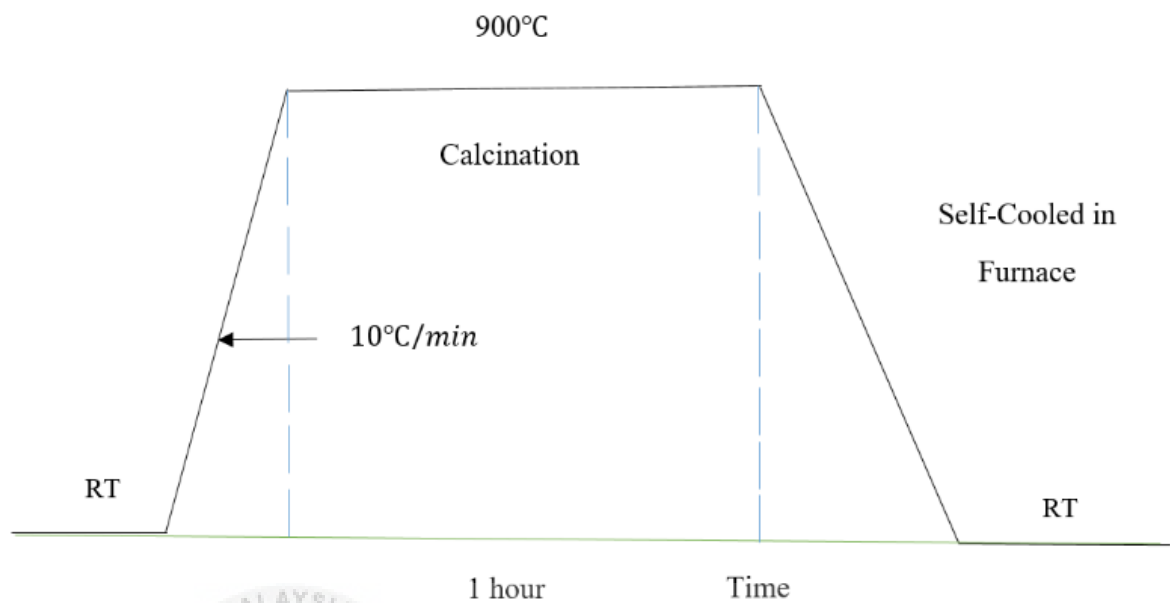


Figure 3.11 Calcination profile of ashes product

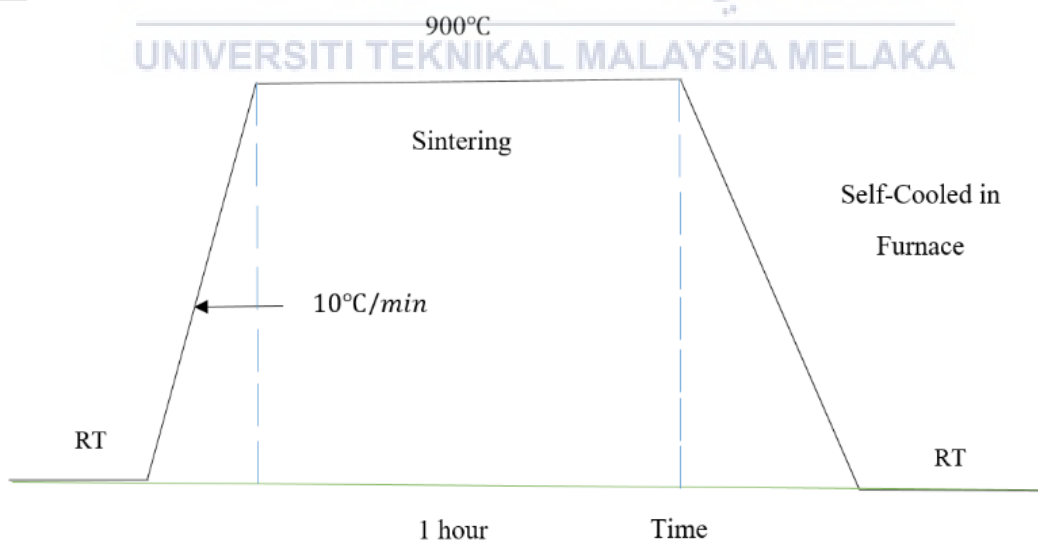
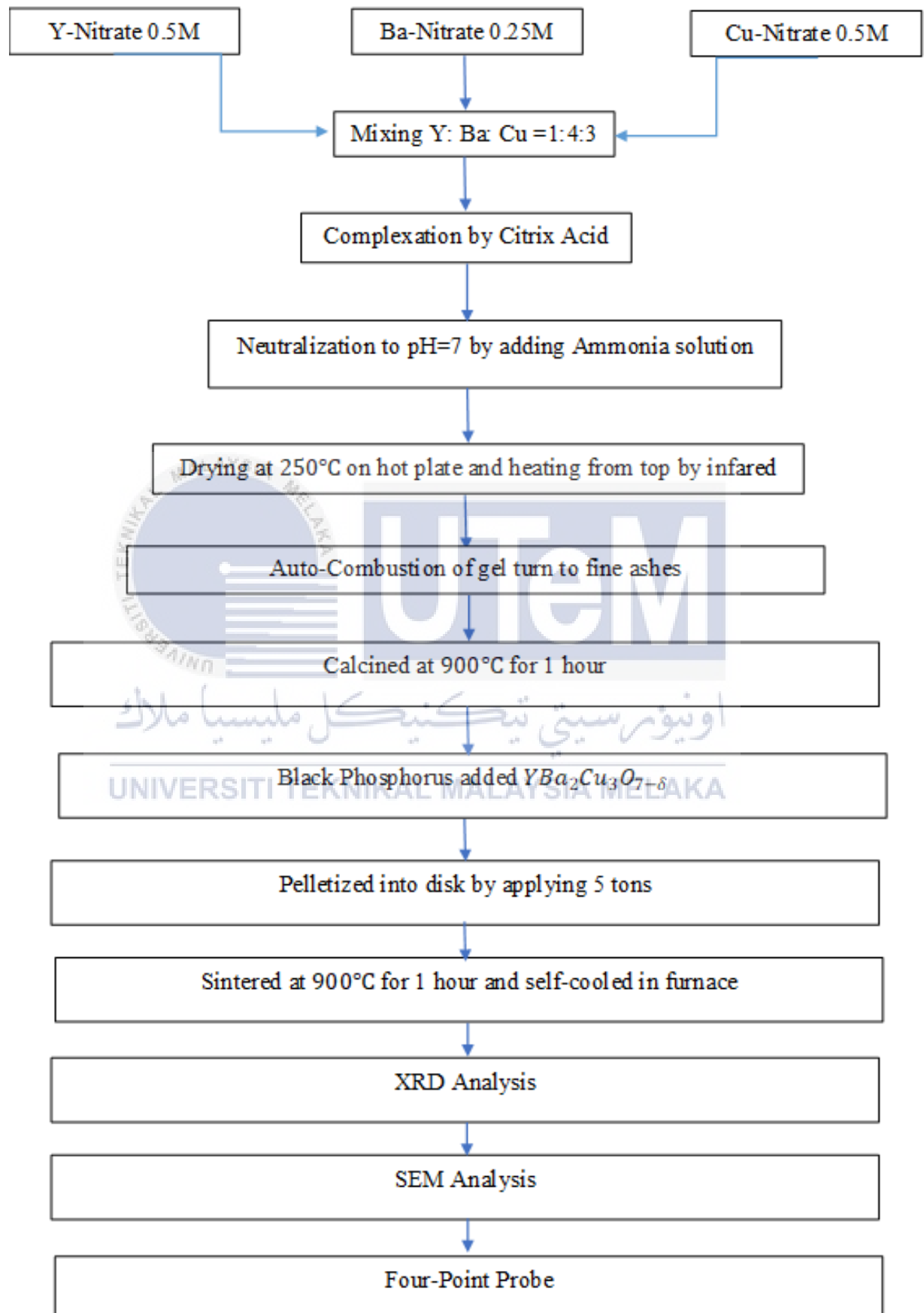


Figure 3.12 Sintering profile of the pellet samples

3.2.6 Process Flow Chart



3.3 Characterization Technique

The structural and superconductivity properties of sample will be characterized by using XRD, SEM and Four-Point Probe.

3.3.1 X-ray Diffraction (XRD)

The crystallographic structure of sample is determined by X-ray diffraction analysis (XRD). XRD can be used to determine the structural properties of nanocomposite. XRD is also performed to analyse any changes in the crystal structure of matrix after adding nanoparticles. The analytical technique of XRD is based on the diffraction of X-rays by matter, particularly for crystalline materials. These X-rays are produced by a cathode ray tube which is then filtered to produce monochromatic radiation, collimated to concentrate and directed toward the sample. The interaction of the incident rays with sample produced constructive interference when conditions satisfied Bragg's Law,

$$n\lambda = 2d \sin \theta \quad \text{Equation 4.0}$$

Where d is the spacing between diffracting planes, θ is the incident angle, n is an integer and λ is the beam wavelength.

The geometry of an X-ray diffractometer is that sample rotated at an angle θ in the direction of collimated X-ray beam, while the X-ray detector is positioned on an arm that rotated at angle of 2θ to collect the diffracted X-rays. The X-ray signal is recorded and processed by a detector and converted the signal to a count rate which is then sent to a device such as computer monitor.

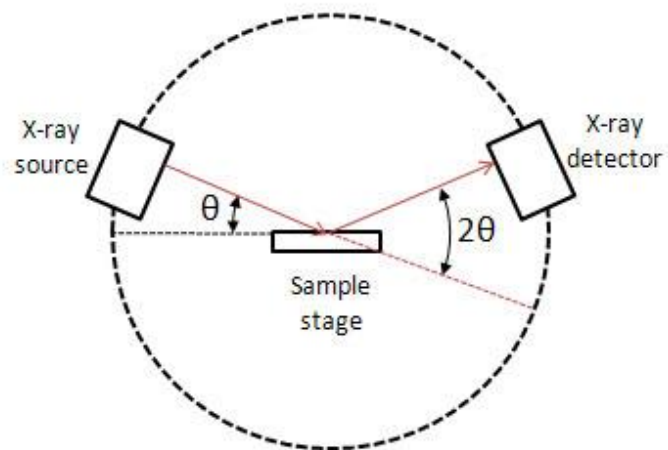


Figure 3.13 Schematic diagram of a diffractometer system



Figure 3.14 XRD Machine

3.3.2 Scanning Electron Microscope (SEM)

The microstructure of sample was observed using Scanning Electron Microscope (SEM). An SEM is a type of microscope that created a high resolution image by scanning the surface of sample with a focused beam of electrons. SEM is one of the most prevalent technologies for examining the microstructure and morphology of materials. The process begins with an electron being created and fired using electron guns which accelerates down the microscope, passing through a sequence of lenses and apertures to form a focused beam that interacts with the surface of sample. The sample is placed on stage in the chamber of microscope. The scan coils controlled the position of electron beam above the objective lens and these coils allow the beam to scan across the sample surface which allows information on a particular area to be collated. The interaction between the sample and the electron produced signals which are subsequently detected by detectors. Then, images are created by detector and presented on a computer screen.

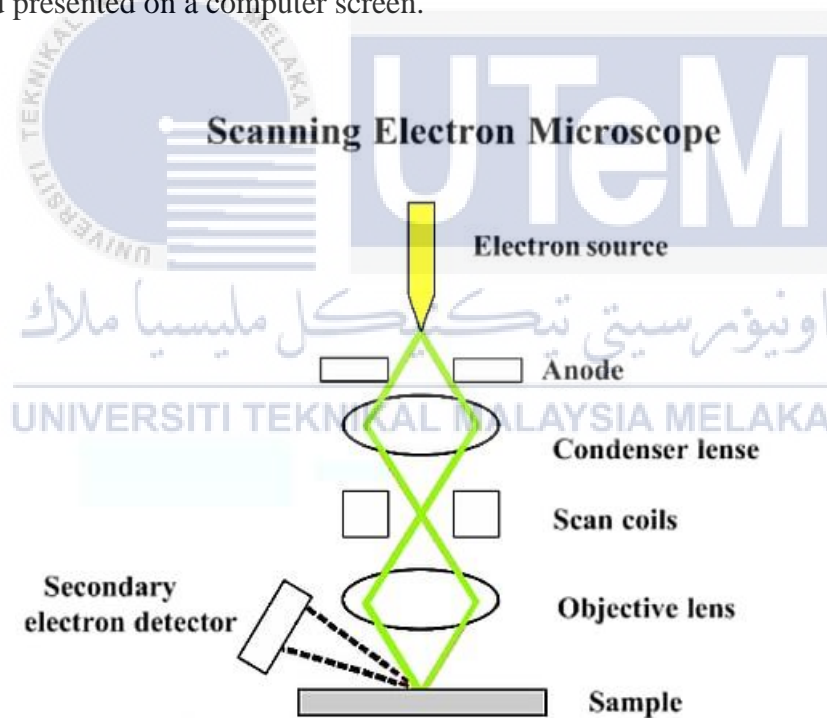


Figure 3.15 Basic components of an SEM



Figure 3.16 Scanning Electron Microscope (SEM)

3.3.3 Resistivity-Temperature (R-T) Measurement by Four-Point Probe

A typical D.C four-point probe was used to measure the resistance across the sample. The resistance with respect to the temperature was examined to identify critical temperature, T_c of sample. This method has four points that make contact with sample surface. These four probes are designed to be lined up in a straight line with spacing between them fixed in such way so that each probe is the same distance apart. The potential difference across the resistor between probe 2 and probe 3 (inner probes) is measured where the current supply pass through probe 1 and probe 4 (outer probes). This method is frequently used to examine the electric properties of material. Figure 3.6 show the schematic diagram of a four-point probe.

The sample was cooled with liquid nitrogen at 77K. The coolant was poured into a dewar with the sample immersed completely until thermal equilibrium was achieved. The sample was raised above the surface of liquid nitrogen and allowed to warm up thereby controlling resistance and temperature of the superconductor. Then, the respective measurement was recorded. The measured temperature was determined using a thermocouple. The sample is firstly cooled down then the temperature was gradually raised

to the required temperature using a temperature controller thereby taking its respective resistance value. Based on these measurements, the R-T characteristics curve were plotted.



Figure 3.17 Four-Point Probe

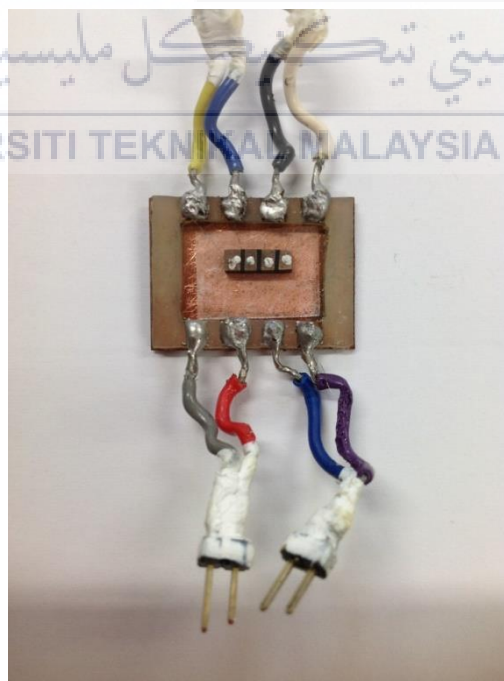


Figure 3.18 Sample holder set up
for resistivity measurement

CHAPTER 4

RESULTS AND DISCUSSION

This chapter presents the results and discussion on decomposition characteristics, structural and superconductivity properties of $YBa_2Cu_3O_{7-x}$ added black phosphorus.

4.1 Structural Properties of $YBa_2Cu_3O_{7-\delta}$

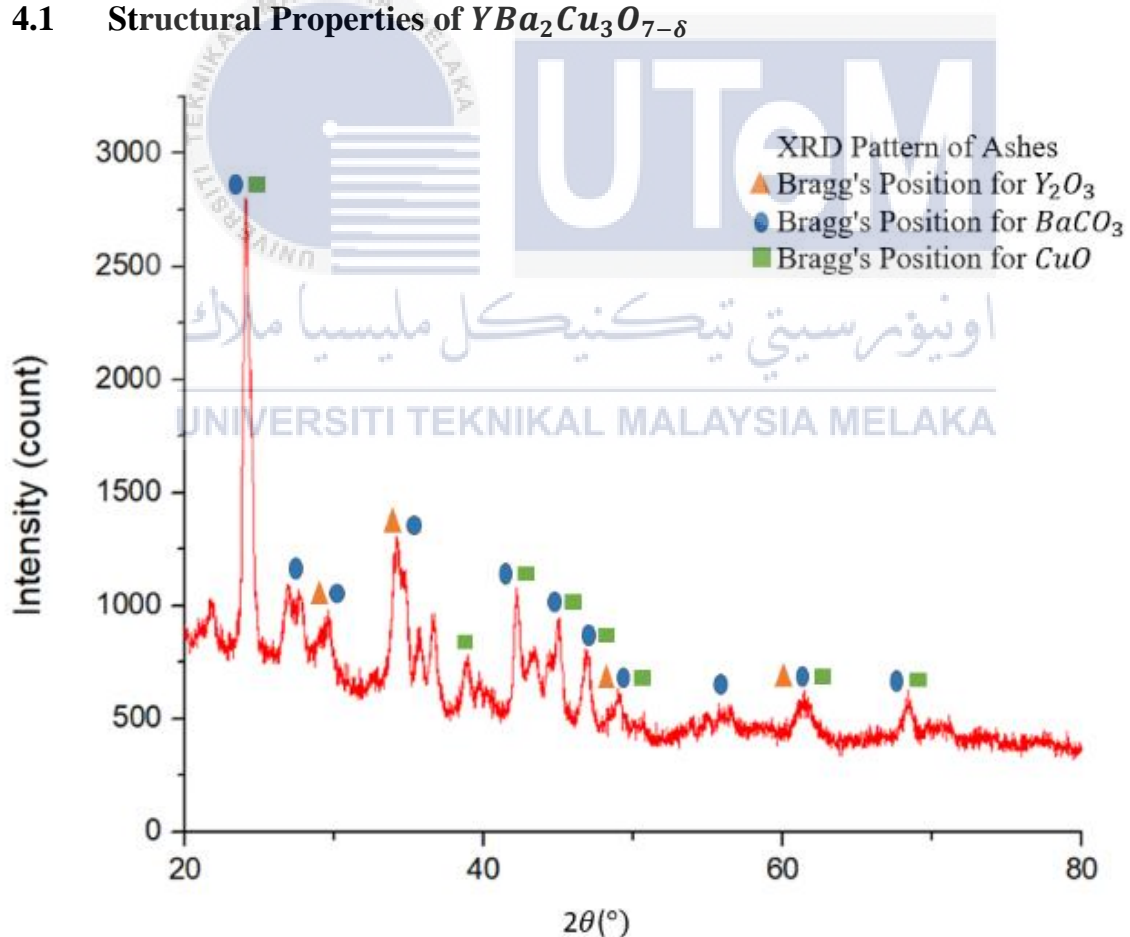
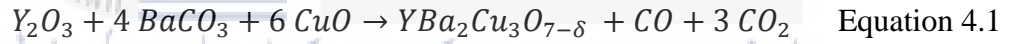


Figure 4.1 XRD patterns of ashes sample before calcination

Figure 4.1 shows the ashes sample before calcination. It revealed that the ashes sample had amorphous structure. The ashes sample contained Y_2O_3 , $BaCO_3$, and CuO as most of the peaks were assigned to Bragg's diffraction position of these compounds. These assigned peaks were indicated by orange triangle, blue circle and green square dots for Y_2O_3 , $BaCO_3$, and CuO compounds respectively. However, there is still a lot of un-assigned peaks show in the figure which indicate the existence of impurities. These impurities may be consisted of citrate ashes or undecomposed substances. These impurities were eliminated during calcination process which will produced high crystalline and pure $YBa_2Cu_3O_{7-\delta}$ sample as depicted by XRD pattern in Figure 4.2

XRD pattern in Figure 4.2 shows the powder sample after calcination. It is believed that calcination process at 900°C for 1 hour is sufficient to yield high crystallinity in $YBa_2Cu_3O_{7-\delta}$ phase. Calcination process is able to eliminate the unwanted impurities in the ashes then formed pure $YBa_2Cu_3O_{7-\delta}$ phase. The equation invloved in calcination process is shown as below,



From the equation (4.1), it revealed that the purity of resultant $YBa_2Cu_3O_{7-\delta}$ is depended on the expected mole of Y_2O_3 , $BaCO_3$, and CuO in the ashes. From the previous dicussion, the amount of moles of Y_2O_3 , $BaCO_3$, and CuO ashes can only be achieved by the complete decomposition of Y, Ba, and Cu nitrated through citrate-nitrate auto-combustion.

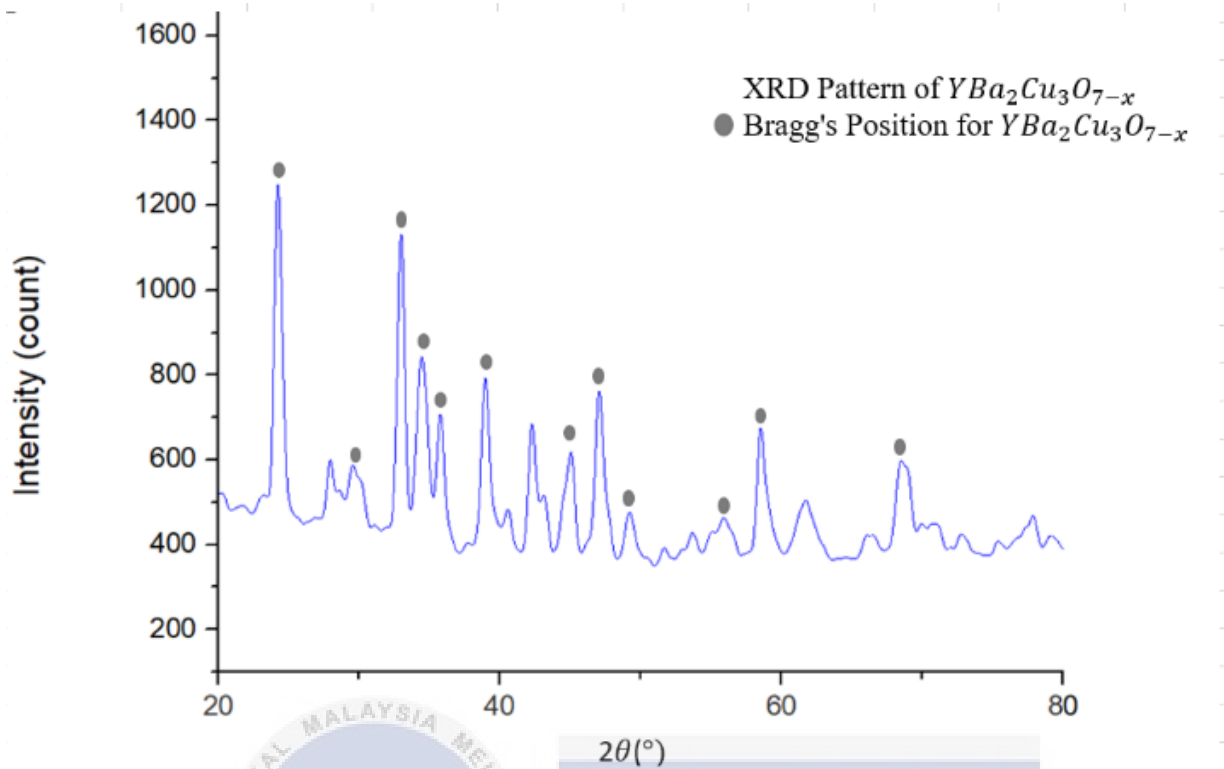


Figure 4.2 XRD pattern of powder sample after calcination

Figure 4.3 The XRD patterns demonstrated specific peaks for YBCO added 0% wt of Black Phosphorus after sintered for 1 hour at 900°C. The XRD pattern indicated that this sample contained high crystalline pure $YBa_2Cu_3O_{7-\delta}$ phase. Hence, the differences of intensity were attribute from the alteration of structural parameters of the sample. The intensity difference patterns for various composition of Black Phosphorus added $YBa_2Cu_3O_{7-\delta}$ samples are shown in Figure 4.4.

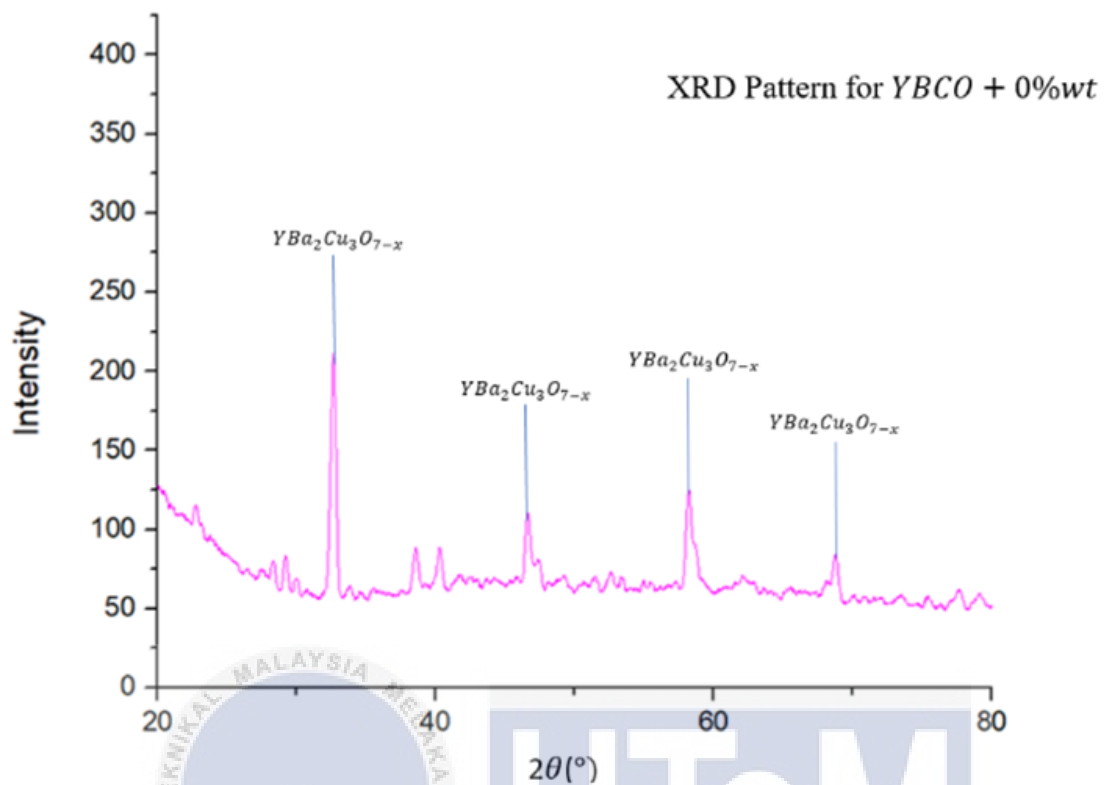


Figure 4.3 Refined XRD pattern of sample without black phosphorus ($x=0\%$ wt)

Figure 4.4 shows smooth intensity difference lines with few minor peaks were observed. The presence of superconducting phase $YBa_2Cu_3O_{7-\delta}$ and Black Phosphorus in the composites is verified. This evidence confirmed the existence of crystalline $YBa_2Cu_3O_{7-\delta}$ phase as dominant structure in each sample. The XRD analysis shows highest peak around 32° . It is noticed that there is no considerable changes in the crystalline patterns of diffractions upon the addition of Black Phosphorus, except for extra small peaks found between 27° to 30° . In sample with $x=6, 8, 10\%$ wt, the existence of Black Phosphorus is confirmed in sample due to having significant peak in XRD pattern. This could be due to high intensity of Black Phosphorus peaks. Additionally, impurities might be existed in these samples since it contained few peaks which were not assigned for $YBa_2Cu_3O_{7-\delta}$ or Black Phosphorus detected at around $20^\circ - 29^\circ$ especially for samples containing higher amount of Black Phosphorus such as $x=8\%$ wt and $x=10\%$ wt.

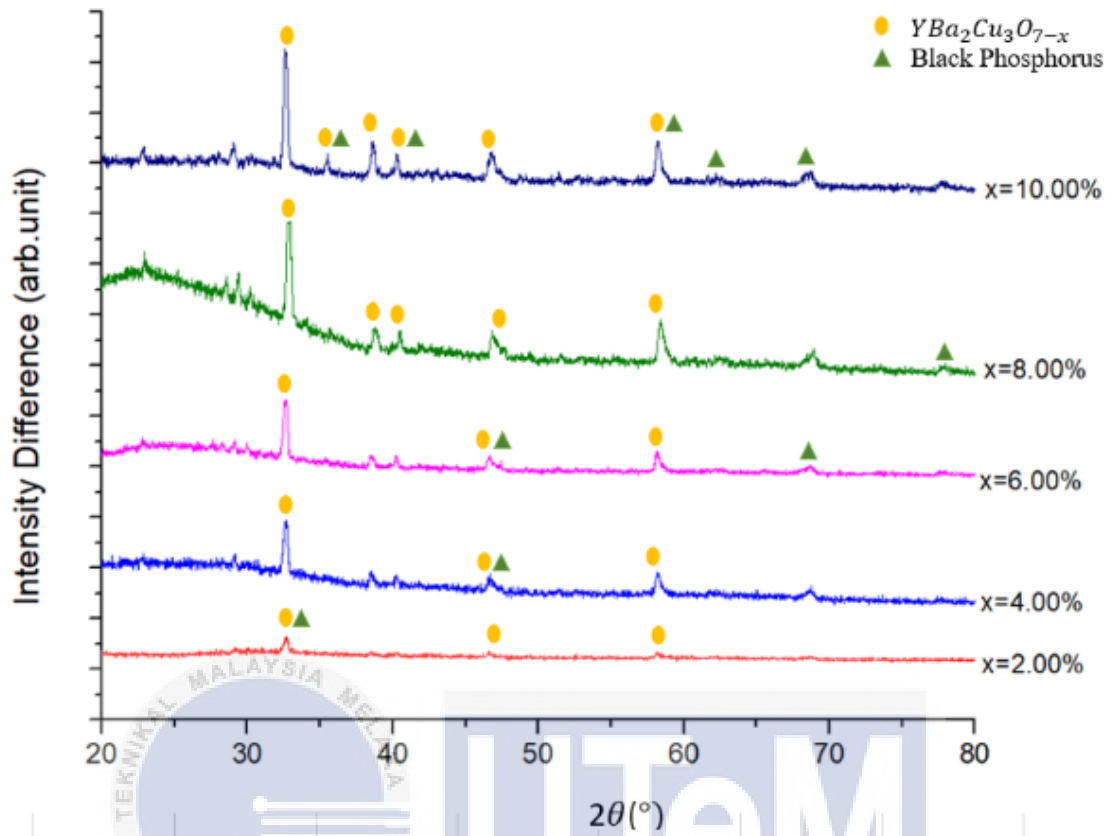


Figure 4.4 Intensity differences patterns for various composition of black phosphorus nanoparticles added $YBa_2Cu_3O_{7-\delta}$ samples.

4.2 Microstructure of Black Phosphorus added $YBa_2Cu_3O_{7-\delta}$

The SEM images of as-prepared pellet sample with $x=0,2,4,6,8,10$ % wt are shown in Figures below.

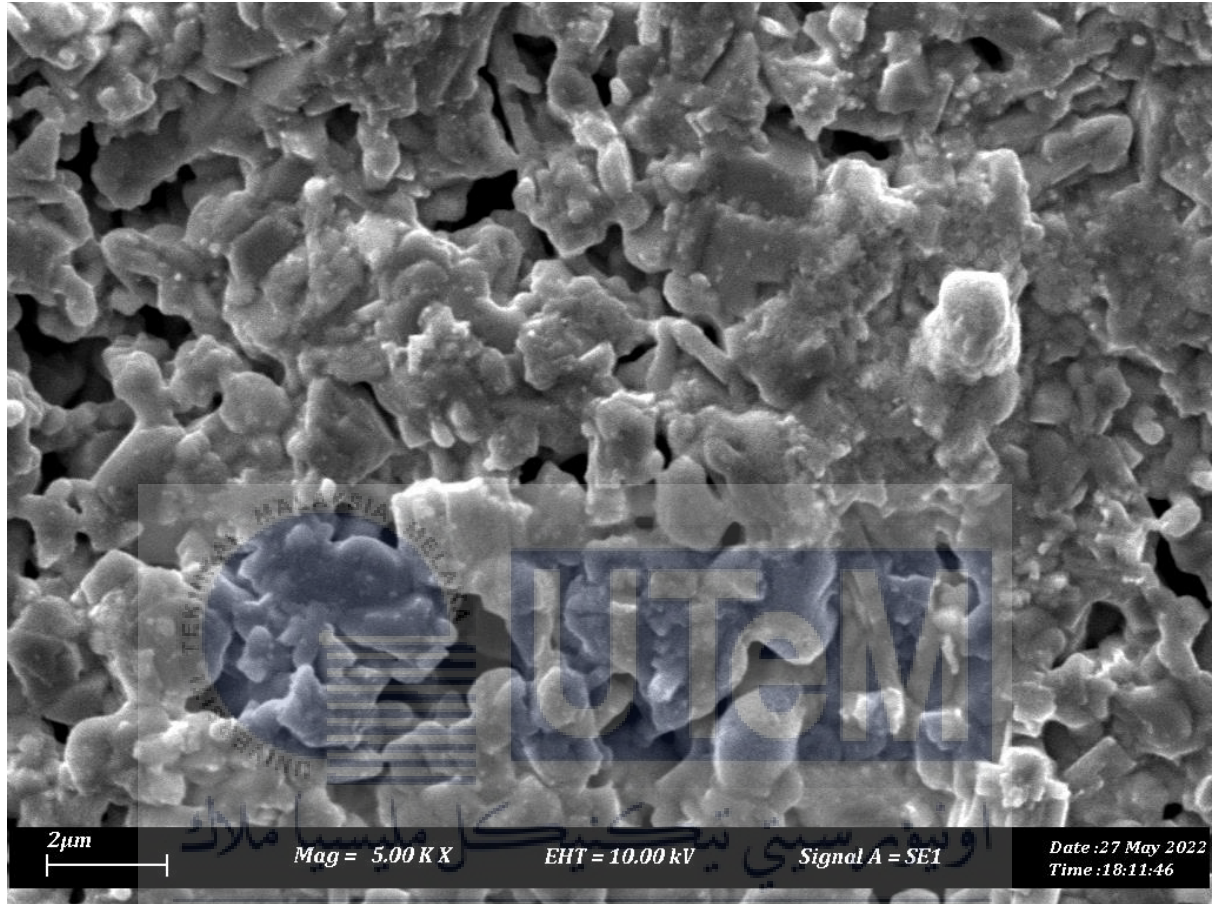


Figure 4.5 SEM image of the sample with $x=0.0\%$

Figure 4.5 shows microstructure of sample with $x=0\%$ wt. It appeared these grains were constructed of particles with melted-like microstructure. It is observed the sample consisted of distinct $YBa_2Cu_3O_{7-\delta}$ particles and pores. These particles were observed connected to each other and shows variation of particle sizes, it developed large gap between the particles which appears as pores. This indicated that the grains of $YBa_2Cu_3O_{7-\delta}$ as just started to grow during heat treatment process.

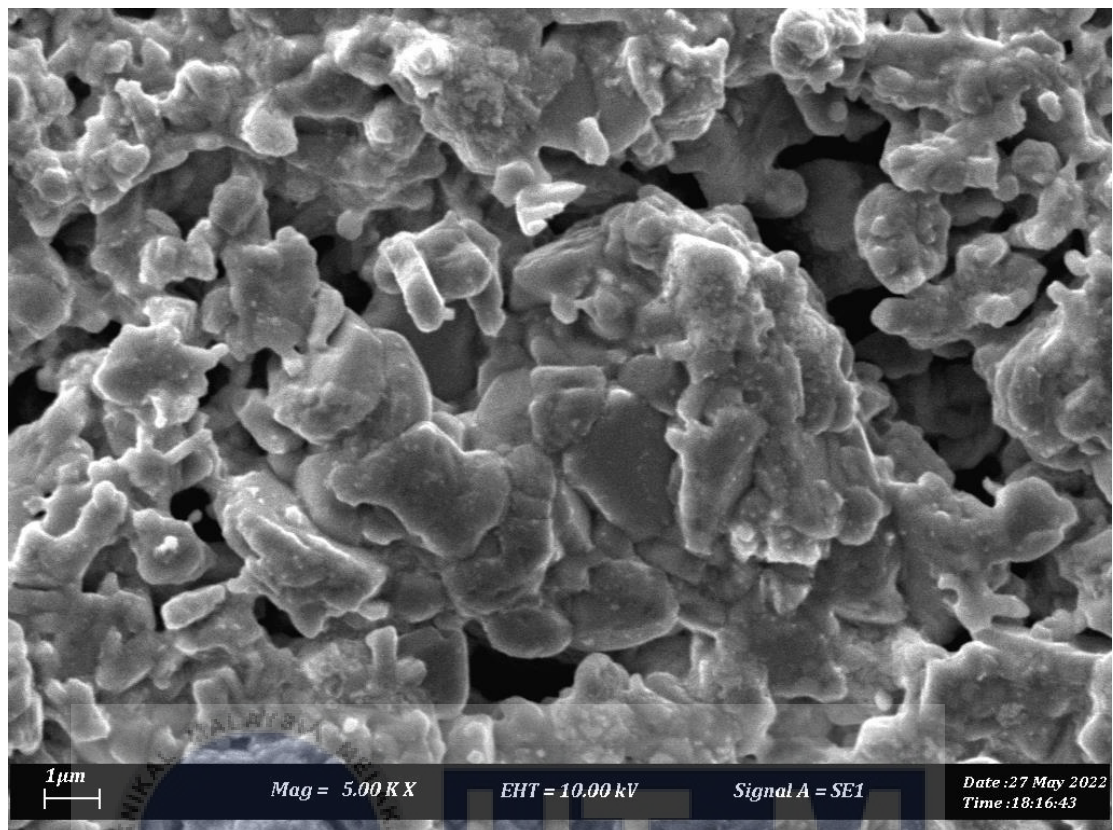


Figure 4.6 SEM image of sample with $x=2.0\%$

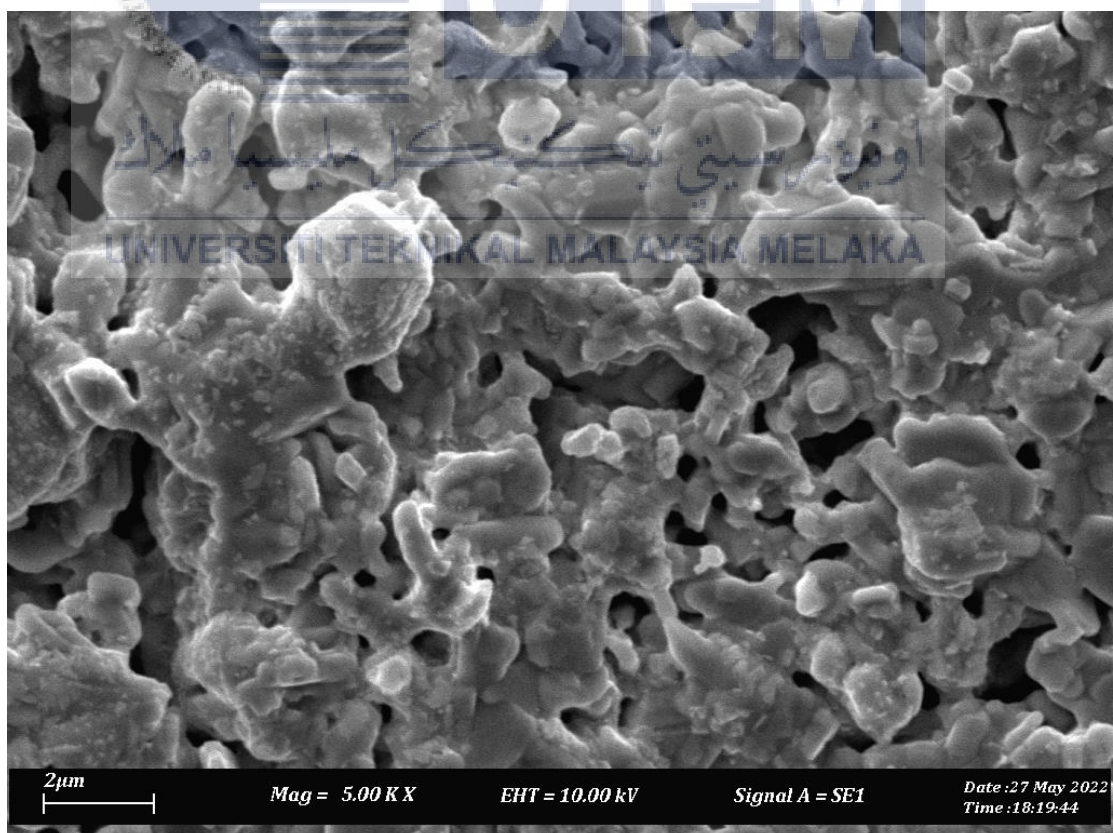


Figure 4.7 SEM image of sample with $x=4.0\%$

Figure 4.6 shows sample with $x=2.0\%$. These particles shows non-uniform shape and less connected to each other. It can be seen in figure the sample shows large gaps among the particles. This type of structure was believed to have low connectivity between particles. Figure 4.7 shows the surface morphology of sample with $x=4.0$ wt%. The morphology could be clearly observed in the images and revealed that there is no significant change in the grain morphology, which was almost similar to $x=2\%$ wt whereas the sample show dense and well-connected grains. This is due to the continuous growth of $YBa_2Cu_3O_{7-\delta}$ grain during calcination followed by heat treatment.

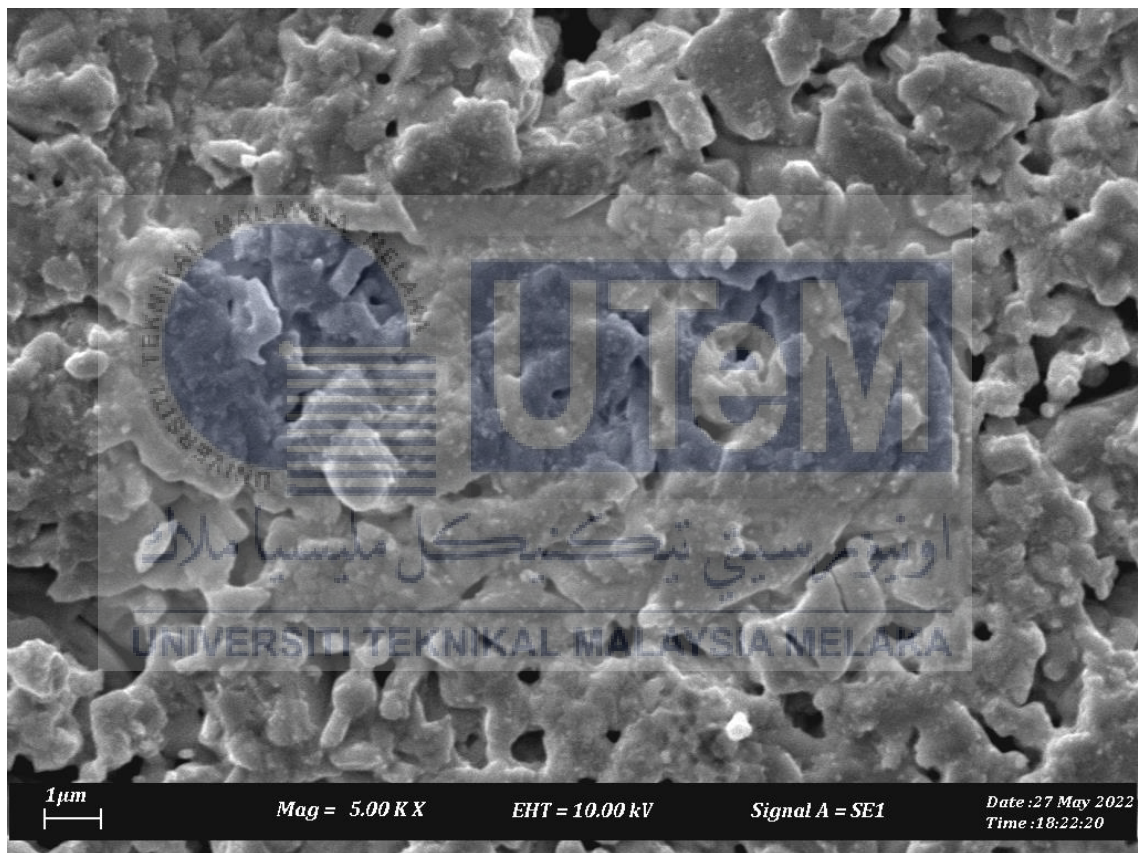


Figure 4.8 SEM image with sample with $x=6.0\%$

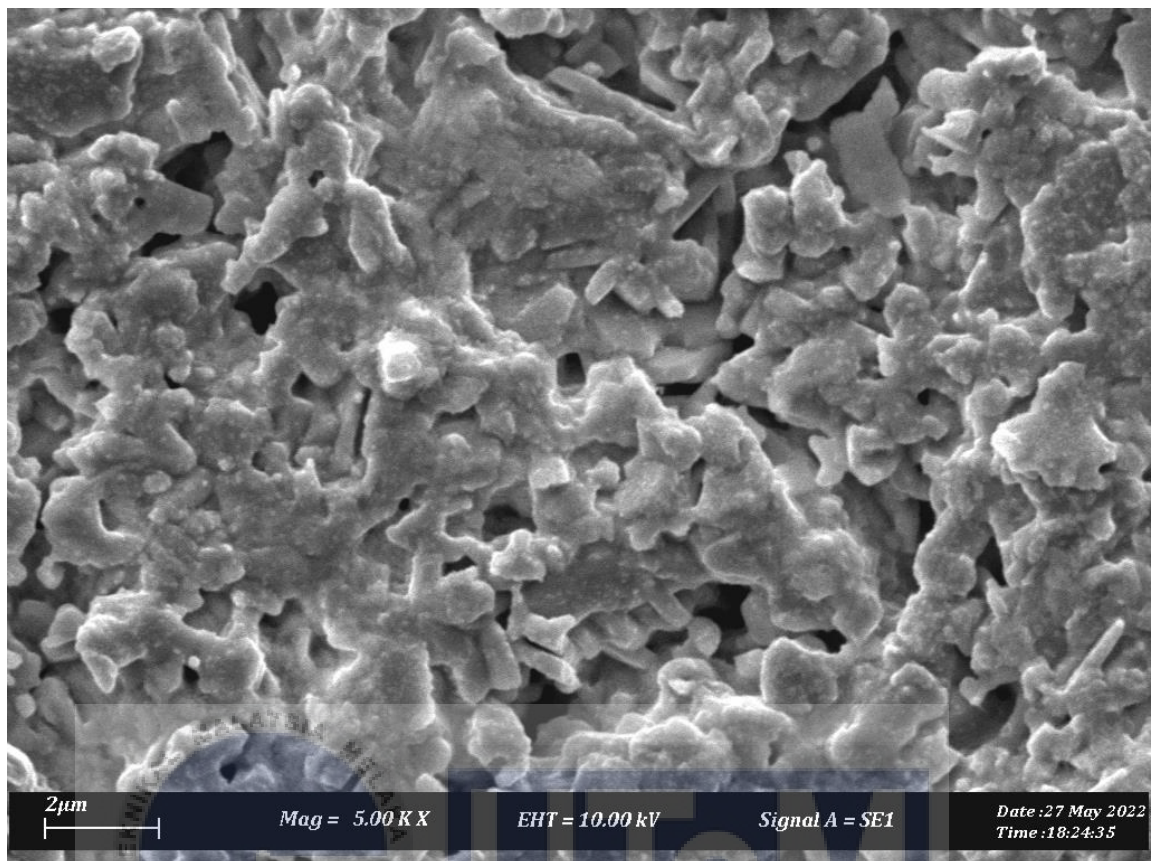


Figure 4.9 SEM image with sample with x=8.0%

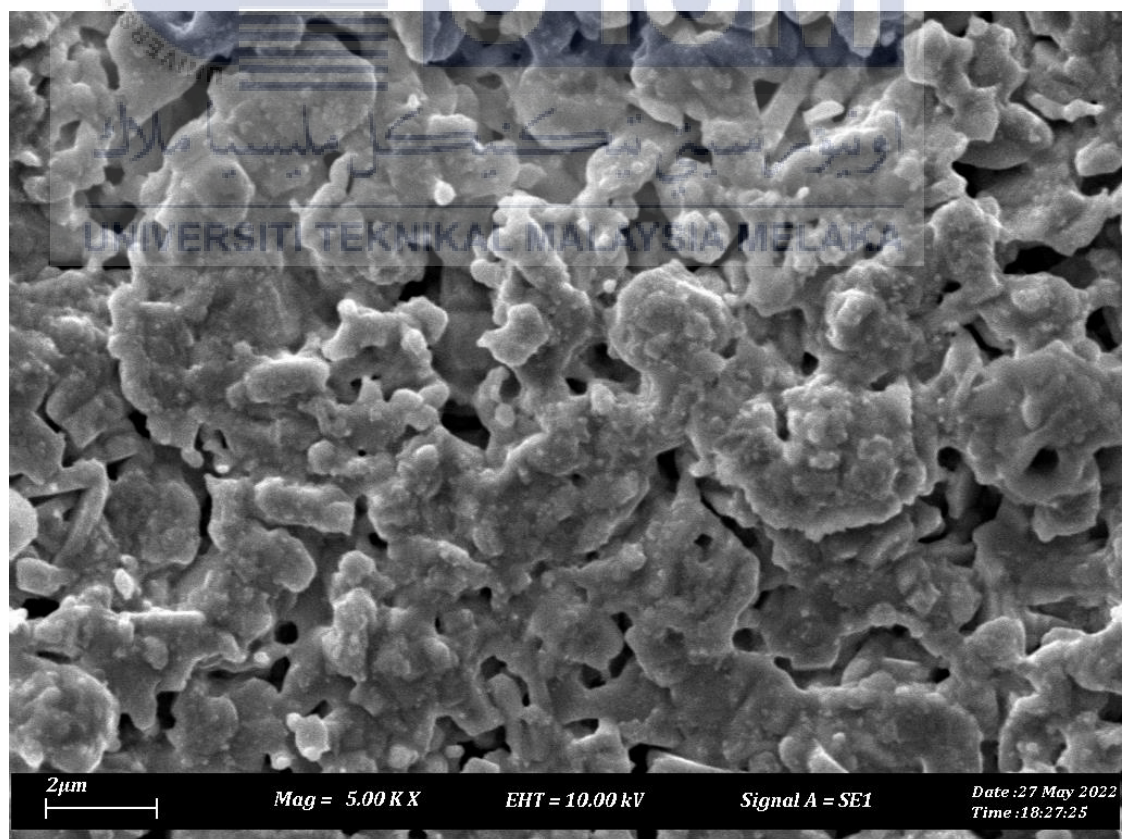


Figure 4.10 SEM image with sample with x=10.0%

Sample with $x=6.0\%$, $x=8\%$ wt, and $x=10.0\%$ wt were observed to have a more compact and more dense structure. It was clearly seen that these samples consisted large number of stacking with relatively irregular structure. Variation of the sizes was attributed from single or multi $YBa_2Cu_3O_{7-\delta}$ grains in the particle. These samples shows less pores due to the grains of $YBa_2Cu_3O_{7-\delta}$ were continued to grow and filled the gap between the particles. This morphological fact could be significant for oxygen diffusion which implying that sample synthesis was performed with the optimal oxygenation. It is believed that the Black Phosphorus nanoparticles were covered by the molten $YBa_2Cu_3O_{7-x}$ structure in the sample. From microstructural observation, it appeared that sample with $x=6.0\%$ have structure with least pores and better grain connectivity due to well distribution of Black Phosphorus nanoparticles.

4.3 Superconducting Properties of $YBa_2Cu_3O_{7-\delta}$

Temperature dependence resistivity of each sample in shown in Figure 4.11

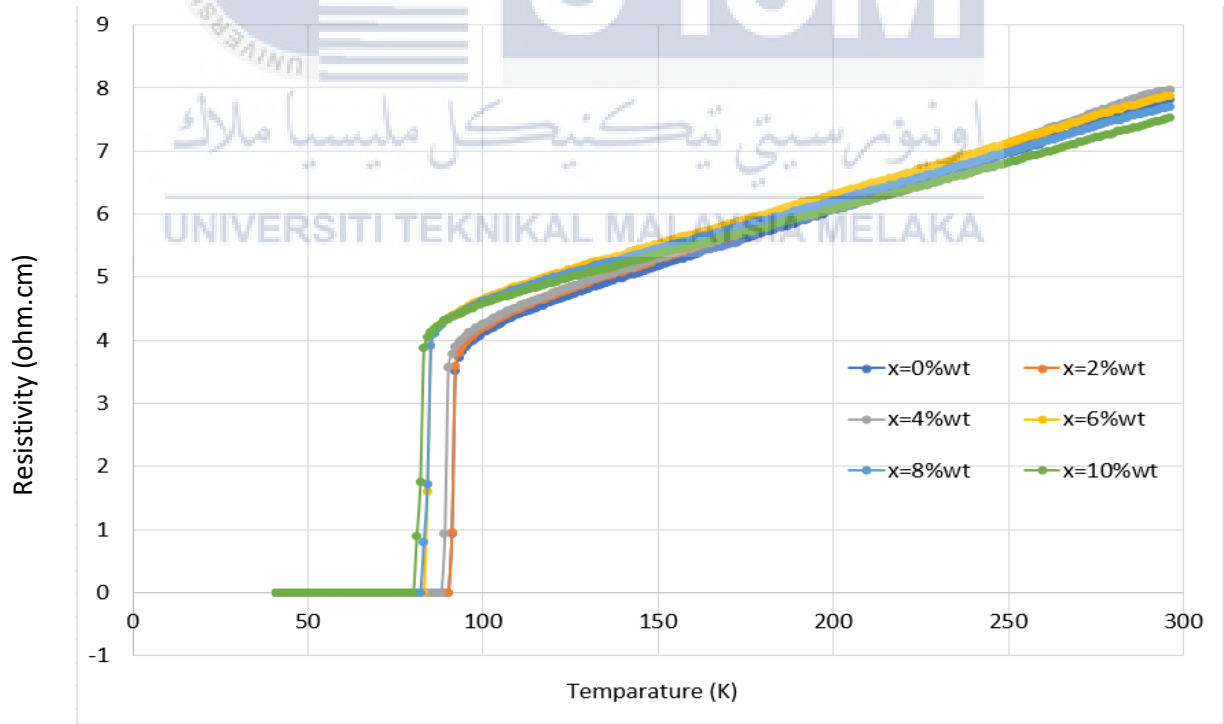


Figure 4.11 Temperature dependence Resistivity of un-Added and Black Phosphorus added $YBa_2Cu_3O_{7-\delta}$ samples.

The figure shows each sample achieved zero electrical resistance by the same pattern. When samples reach around 300K, the resistivity of samples was around 8Ω . The resistivity was constantly reduced as the temperature was decreased and suddenly dropped to zero at respective T_c onset. It was observed this rapid drop was occurred with a narrow temperature width. From this pattern, it was indicated that each sample behaved like a metallic material before transformed to superconducting material after T_c onset. A close observation at the critical temperature was shown in Figure 4.12.

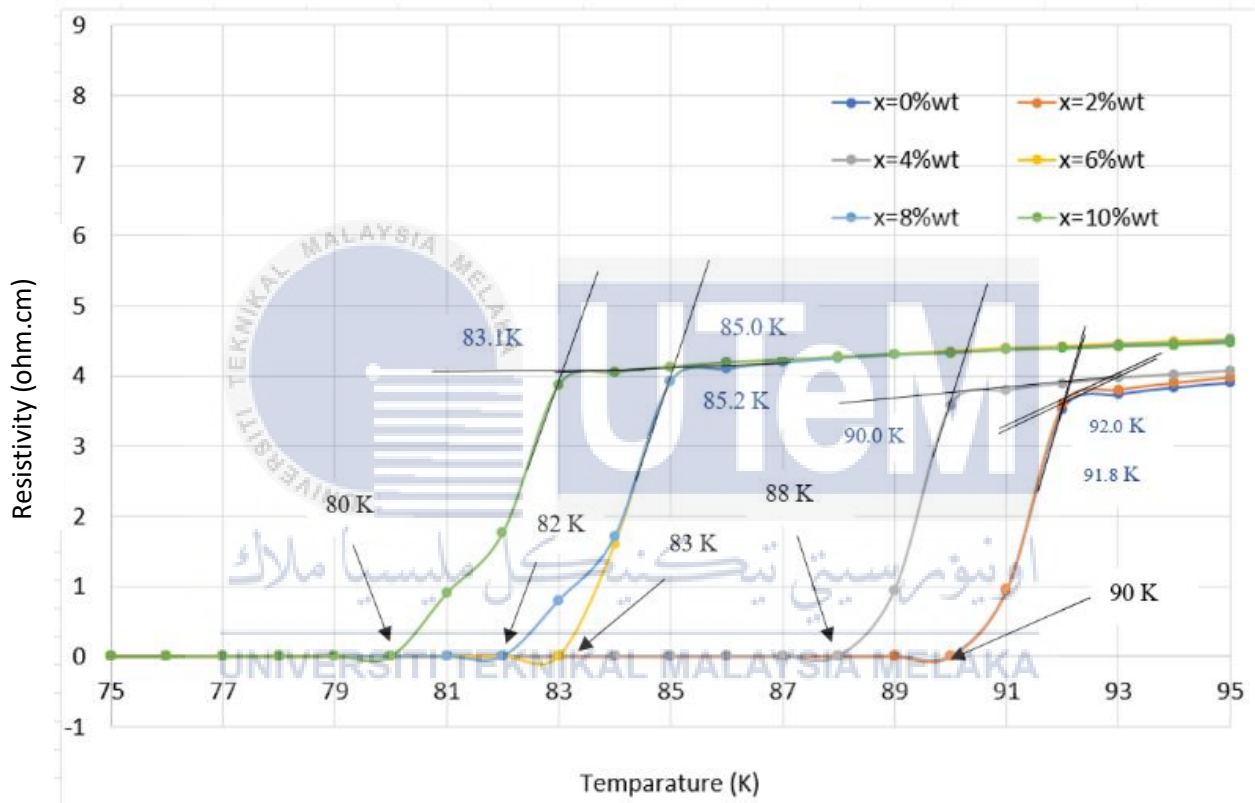
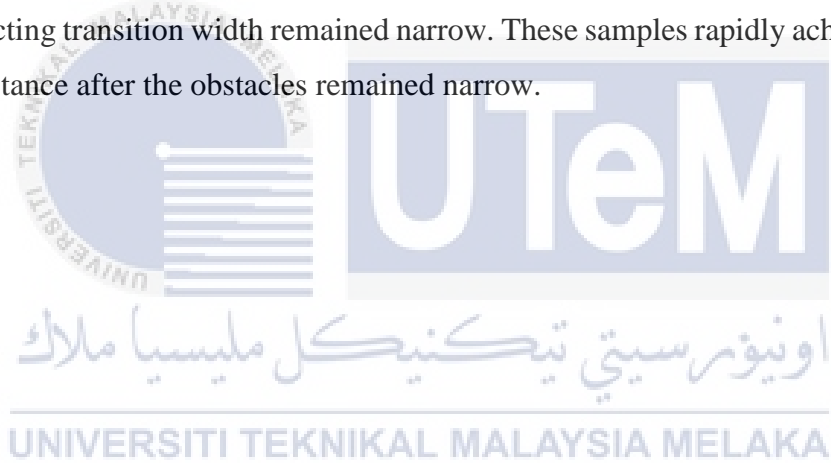


Figure 4.12 Critical Temperatures of un-added Black Phosphorus added $YBa_2Cu_3O_{7-x}$ samples.

Figure 4.9 shows the T_c onset and T_c zero of samples. It appeared that both T_c were decreased when amount of Black Phosphorus nanoparticles increased. The T_c onset for sample with $x=2.0\%$ wt is 91.8 K which appeared to be slightly lowered compared to the pure $YBa_2Cu_3O_{7-\delta}$, $T_c=92.0$ K whereas both samples was observed processed similar T_c zero with 90.0 K. The T_c onset for samples with $x=4,6,8,10\%$ wt were 90.0 K, 85.2 K, 85.0 K and 83.1 K respectively whereas their T_c zero were, 88.0 K, 83.0 K, 82.0 K and 80.0 K.

The T_c of Black Phosphorus added $YBa_2Cu_3O_{7-\delta}$ samples had a decreasing pattern but the T_c was not significantly reduced and in all cases it remained above the liquefy temperature of nitrogen (77K).

Based on the results of the temperature dependence resistivity relationship of sample, it was determined that the T_c of $YBa_2Cu_3O_{7-\delta}$ superconductor was reduced due to the introduction of Black Phosphorus nanoparticles in the samples. The Black Phosphorus nanoparticles are known as non-superconducting material which forbids superconducting electrons to pass through. Existence of Black Phosphorus nanoparticles on $YBa_2Cu_3O_{7-\delta}$ grains may obstructed superconducting electrons to flow smoothly. Therefore, in order to surpass those obstacles to achieve ideal flowing condition, the superconducting electrons were required to lower temperature. Additionally, through this factor lowers the T_c the superconducting transition width remained narrow. These samples rapidly achieved the state of zero resistance after the obstacles remained narrow.



CHAPTER 5

CONCLUSION AND RECOMMENDATION

In this work, Black Phosphorus nanoparticles added into $YBa_2Cu_3O_{7-\delta}$ superconductor was successfully synthesized using standard solid-state reaction. Structural properties and superconducting properties of sample added with different composition of Black Phosphorus ($x=0.0, 2.0, 4.0, 6.0, 8.0, 10.0\%$) were studied. The XRD experiments are performed and the XRD patterns shows the formation of $YBa_2Cu_3O_{7-\delta}$ phase. XRD analysis revealed high crystalline structure of samples after sintered. From SEM analysis shows the samples have melt-like structure, porosity decreased and better grain-connectivity between particles when weight percentage of Black Phosphorus increased. SEM revealed that sample added with $x=6.0\%$ wt of Black Phosphorus has more compact and less pores structure. From R-T graph, it was concluded that with increased in weight percentage of Black Phosphorus into $YBa_2Cu_3O_{7-\delta}$ matrix, the critical temperature, T_c decreased but still remained above the liquefy temperature of nitrogen (77K). This shows that the existence of well distributed Black Phosphorus did not affect the T_c in much extent.

5.1 Recommendation

The success of this research works can be continued with further investigations on the effects of Black Phosphorus nanoparticles towards other properties of the samples such as the magnetic field dependence of transport current density ($J_c - B$ characteristics). These characteristics will help to further understand the mechanisms of superconducting properties of $YBa_2Cu_3O_{7-\delta}$ by the addition of nanoparticles. The suggestion technique will be using magnetic properties measurement system (MPMS) named superconducting quantum interference devices (SQUIDs) which can generate a maximum field up to 1 Tesla at liquid

nitrogen temperature (77K). The in-field transport critical current ($J_c - B$) measurements can be done by this technique. Another characterization technique which is Energy-Dispersive X-ray Spectroscopy (EDX) is suggest to determine the percentage of elements in the sample. It can use to determine that the sample consist of $YBa_2Cu_3O_{7-\delta}$ and Black Phosphorus phases. It also can help to reveal the atomic ratio of Y, Ba, Cu, O and Black Phosphorus elements. Further EDX analysis can provide the evidence of Black Phosphorus nanoparticles.



REFERENCES

- A. N. Jannah, I. Mariana and A. Shanthi (2020). Effects of Ni_2O_3 Addition on $\text{YBa}_2\text{Cu}_3\text{O}_{7-\delta}$ (Ni_2O_3)_x Superconductor. *Malaysian Journal of Chemistry*, Vol. 22 (1), 1-7
- Akimitsu, J. (2019). Towards higher- T_c superconductors. *Proceedings of the Japan Academy, Series B*, 95(7), 321-342.
- Alecu, G. (2004). Crystal structures of some high-temperature superconductors. *Romanian Reports in Physics*, 56(3), 404-412.
- Alotaibi, S.A., Slimani, Y., Hannachi, E., Almessiere, M.A., Yasin, G., Al-qwairi, F.O., Iqbal, M. and Azzouz, F.B., 2021. Intergranular properties of polycrystalline $\text{YBa}_2\text{Cu}_3\text{O}_{7-\delta}$ superconductor added with nanoparticles of WO_3 and BaTiO_3 as artificial pinning centers. *Ceramics International*, 47(24), pp.34260-34268.
- Annabi, M., Bouchoucha, I., Azzouz, F. B., & Salem, M. B. (2010, November). Effect of ZnO and $\text{Zn}_{0.95}\text{Mn}_{0.05}\text{O}$ nano-particle inclusions on YBCO polycrystalline pinning properties. In *IOP Conference Series: Materials Science and Engineering* (Vol. 13, No. 1, p. 012009). IOP Publishing.
- Annabi, M., Bouchoucha, I., Azzouz, F. B., & Salem, M. B. (2010, November). Effect of ZnO and $\text{Zn}_{0.95}\text{Mn}_{0.05}\text{O}$ nano-particle inclusions on YBCO polycrystalline pinning properties. In *IOP Conference Series: Materials Science and Engineering* (Vol. 13, No. 1, p. 012009). IOP Publishing.
- Arlina, A., Karim, Y., Chen, S. K., Halim, S. A., & Kechik, M. A. (2016). Synthesis and Effect of Al_2O_3 Added in Yttrium Barium Copper Oxide $\text{YBa}_2\text{Cu}_3\text{O}_7$ by Solid State Reaction Method. *Journal of Tropical Resources and Sustainable Science (JTRSS)*, 4(2), 75-77.

- Arlina, A., Karim, Y., Chen, S. K., Halim, S. A., & Kechik, M. A. (2016). Synthesis and Effect of Al_2O_3 Added in Yttrium Barium Copper Oxide $\text{YBa}_2\text{Cu}_3\text{O}_{7-\delta}$ by Solid State Reaction Method. *Journal of Tropical Resources and Sustainable Science (JTRSS)*, 4(2), 75-77.
- Attaf, S., Mosbah, M. F., Vecchione, A., & Fittipaldi, R. (2012). The influence of doping with Ca and Mg in $\text{YBa}_2\text{Cu}_3\text{O}_{7-\delta}$ ceramic. In *EPJ Web of Conferences* (Vol. 29, p. 00003). EDP Sciences.
- Bala, A. A., Adam, M. L., Abdullahi, S. S., Musa, I. M., & Adamu, B. I. Determination of YBCO Superconductor Critical Temperature and its Voltage-Current Characteristics using Four-Point Probe Method..
- Bao, T. N., Tegus, O., & Jun, N. (2018). Preparation of black phosphorus by the mechanical ball milling method and its characterization. In *Solid State Phenomena* (Vol. 271, pp. 18-22). Trans Tech Publications Ltd.
- Bennemann, K. H., & Ketterson, J. B. (2008). History of superconductivity: Conventional, high-transition temperature and novel superconductors. In *Superconductivity* (pp. 3-26). Springer, Berlin, Heidelberg.
- Bennemann, K. H., & Ketterson, J. B. (2008). History of superconductivity: Conventional, high-transition temperature and novel superconductors. In *Superconductivity* (pp. 3-26). Springer, Berlin, Heidelberg.
- Beyers, R., & Shaw, T. M. (1989). The Structure of $\text{YBa}_2\text{Cu}_3\text{O}_{7-\delta}$ and its Derivatives. *Solid state physics*, 42, 135-212.
- Bunaciu, A. A., UdrişTioiu, E. G., & Aboul-Enein, H. Y. (2015). X-ray diffraction: instrumentation and applications. *Critical reviews in analytical chemistry*, 45(4), 289-299.
- Cano, D., Kasch, B., Hattermann, H., Kleiner, R., Zimmermann, C., Koelle, D., & Fortágh, J. (2008). Meissner effect in superconducting microtraps. *Physical review letters*, 101(18), 183006.

- Cho, S. J., Uddin, M. J., & Alaboina, P. (2017). Review of nanotechnology for cathode materials in batteries. In *Emerging nanotechnologies in rechargeable energy storage systems* (pp. 83-129). Elsevier.
- Choudhary, O. P., & Choudhary, P. (2017). Scanning electron microscope: advantages and disadvantages in imaging components. *Int. J. Curr. Microbiol. Life Sciences Leaflets*, 85, 1-to.
- Colie, M., Mihaiescu, D. E., Surdu, A., Fikai, A., TRUȘCĂ, R., Istrati, D., & Andronesu, E. (2015). Obtaining $\text{YBa}_2\text{Cu}_3\text{O}_{7-\delta}$ through a modified auto-combustion reaction with and without addition of organic fuel. *Revue Roumaine De Chime*, 60(11-12), 1117-1123.
- Cyrot, M. (1973). Ginzburg-Landau theory for superconductors. *Reports on Progress in Physics*, 36(2), 103.
- De Keukeleere, K., Cayado, P., Meledin, A., Vallès, F., De Roo, J., Rijckaert, H., ... & Van Driessche, I. (2016). Superconducting $\text{YBa}_2\text{Cu}_3\text{O}_{7-\delta}$ nanocomposites using preformed ZrO_2 nanocrystals: growth mechanisms and vortex pinning properties. *Advanced Electronic Materials*, 2(10), 1600161.
- El Bourakadi, K., & Bouhfid, R. (2021). Characterization techniques for hybrid nanocomposites based on cellulose nanocrystals/nanofibrils and nanoparticles. In *Cellulose Nanocrystal/Nanoparticles Hybrid Nanocomposites* (pp. 27-64). Woodhead Publishing.
- Farbod, M., & Batvandi, M. R. (2011). Doping effect of Ag nanoparticles on critical current of $\text{YBa}_2\text{Cu}_3\text{O}_{7-\delta}$ bulk superconductor. *Physica C: Superconductivity*, 471(3-4), 112-117.
- Gapud, A. A, Kumar. D, Viswanathan, S. K, Cantoni.C., Varela. M., Abiade.J & Christen.D. K. (2005). Enhancement of flux pinning in $\text{YBa}_2\text{Cu}_3\text{O}_{7-\delta}$ thin films embedded with epitaxially grown Y_2O_3 nanostructures using a multi-layering process. *Superconductor Science and Technology*, 18(11), 1502.
- Ghattas, A., Annabi, M., Zouaoui, M., Azzouz, F. B., & Salem, M. B. (2008). Flux pinning by Al-based nano particles embedded in polycrystalline (Bi,Pb)-2223 superconductors. *Physica C: Superconductivity and its applications*, 468(1), 31-38.

- Giri, R., Awana, V. P. S., Singh, H. K., Tiwari, R. S., Srivastava, O. N., Gupta, A., ... & Kishan, H. (2005). Effect of Ca doping for Y on structural/microstructural and superconducting properties of $\text{YBa}_2\text{Cu}_3\text{O}_{7-\delta}$. *Physica C: Superconductivity and its applications*, 419(3-4), 101-108
- Grosche, F., 2004. Superconductivity. *Science Progress*, 87(1), pp.51-78.
- Istrate, N. (2014) Determining the critical temperature of YBaCu_3O_7 superconductor by using a four-point probe and type-T thermocouple.
- Karakaya, S., Akarsu, M., Aydoğu, S., & Özbaş, Ö. (2010). Properties of vortex states in high temperature superconductors. *Journal of Science and Technology of Dumlupınar University*, (023), 11-22.
- Kozuka, H., Umeda, T., Jin, J., Monde, T., & Sakka, S. (1988). Application of Sol-Gel Processing to Preparation of High Temperature Superconducting Materials. *Bulletin of the Institute for Chemical Research, Kyoto University*, 66(2), 80-92.
- Landínez-Téllez, D. A., Roa-Rojas, J., & Peña-Rodríguez, G. (2013). Structural and magnetic properties of $\text{YBa}_2\text{Cu}_3\text{O}_7 / \text{BaZrO}_3$ composites. *Materials Research*, 16, 1002-1005.
- Li, D. H., He, S. F., Chen, J., Jiang, C. Y., & Yang, C. (2017, September). Solid-state chemical reaction synthesis and characterization of lanthanum tartrate nanocrystallites under ultrasonication spectra. In *IOP Conference Series: Materials Science and Engineering* (Vol. 242, No. 1, p. 012023). IOP Publishing
- Li, Z., Coll, M., Mundet, B., Chamorro, N., Vallès, F., Palau, A., Gazquez, J., Ricart, S., Puig, T. and Obradors, X., 2019. Control of nanostructure and pinning properties in solution deposited $\text{YBa}_2\text{Cu}_3\text{O}_{7-x}$ nanocomposites with preformed perovskite nanoparticles. *Scientific reports*, 9(1), pp.1-14.
- Liu, H., Du, Y., Deng, Y. and Peide, D.Y., 2015. Semiconducting black phosphorus: synthesis, transport properties and electronic applications. *Chemical Society Reviews*, 44(9), pp.2732-2743.
- Liu, Y., Cui, D., Chen, M., Li, Z., & Zhou, C. (2019). Synthesis of Red and Black Phosphorus Nanomaterials. In *Fundamentals and Applications of Phosphorus Nanomaterials* (pp. 1-25). American Chemical Society.

- Lundy, D. R., Swartzendruber, L. J., & Bennett, L. H. (1989). A brief review of recent superconductivity research at NIST. *Journal of research of the national institute of standards and technology*, 94(3), 147.
- M. Annabi, O. Zayed, M. Fteiti and M. Aouissi (2020). Microstructure and normal state properties for YBCO system added by $\text{Zn}_{0.95}\text{Fe}_{0.05}\text{O}$ nanoparticles. *Multi-Knowledge Electronic Comprehensive Journal For Education And Science Publications (MECSJ)*. 2616-9185.
- Malmivirta, M., Rijckaert, H., Paasonen, V., Huhtinen, H., Hynninen, T., Jha, R., ... & Paturi, P. (2017). Enhanced flux pinning in YBCO multilayer films with BCO nanodots and segmented BZO nanorods. *Scientific reports*, 7(1), 1-8.
- Maruyama, Y., Suzuki, S., Kobayashi, K., & Tanuma, S. (1981). Synthesis and some properties of black phosphorus single crystals. *Physica B+ c*, 105(1-3), 99-102.
- Pandey, A., Nikam, A.N., Fernandes, G., Kulkarni, S., Padya, B.S., Prassl, R., Das, S., Joseph, A., Deshmukh, P.K., Patil, P.O. and Mutalik, S., 2021. Black phosphorus as multifaceted advanced material nanoplatfroms for potential biomedical applications. *Nanomaterials*, 11(1), p.13.
- Piras, C. C., Fernández-Prieto, S., & De Borggraeve, W. M. (2019). Ball milling: a green technology for the preparation and functionalisation of nanocellulose derivatives. *Nanoscale Advances*, 1(3), 937-947.
- Prabhakar, B., & Wani, T. A. (2020, October). Crystal structure visualization and powder diffraction pattern of YBCO superconductor. In *AIP Conference Proceedings* (Vol. 2281, No. 1, p. 020003). AIP Publishing LLC.
- R. Aima1, S. A. Halim, S. K. Chen, and M. M. Awang Kechik (2018). The Effect Of Sm_2O_3 Nanoparticle Inclusion On Superconducting Properties Of YBCO Ceramics, *ASM Science Journal Special Issue*. Ramli, A., Shaari, A. H., Baqiah, H., Kean, C. S., Kechik, M. M. A., & Talib, Z. A. (2016). Role of Nd_2O_3 nanoparticles addition on microstructural and superconducting properties of $\text{YBa}_2\text{Cu}_3\text{O}_{7-\delta}$ ceramics. *Journal of Rare Earths*, 34(9), 895-900.
- Rani, P., & Saxena, P. (2019). Structural Characterization of Iron Doped Layered YBCO Superconductor. *Journal of Integrated Science and Technology*, 7(1), 14-18.

- Rey, C. M., & Malozemoff, A. P. (2015). Fundamentals of superconductivity. In *Superconductors in the Power Grid* (pp. 29-73). Woodhead Publishing.
- Rodriguez, J., & Lazo, A. (2018, December). Synthesis of YBCO superconductor by the method of combustion reaction in solution. In *Journal of Physics: Conference Series* (Vol. 1143, No. 1, p. 012029). IOP Publishing.
- Shen, B. (2020). *Study of second generation high temperature superconductors: electromagnetic characteristics and AC loss analysis*. Springer Nature.
- Matsushita, T. (2007). Flux pinning in superconductors (Vol. 164). Berlin: Springer.
- Slimani, Y., Almessiere, M. A., Hannachi, E., Mumtaz, M., Manikandan, A., Baykal, A., & Azzouz, F. B. (2019). Improvement of flux pinning ability by tungsten oxide nanoparticles added in $\text{YBa}_2\text{Cu}_3\text{O}_y$ superconductor. *Ceramics International*, 45(6), 6828-6835.
- Subedi, M. S. (2017). Superconductivity and Cooper Pairs. *Himalayan Physics*, 104-107.
- Tinkham, M. (2004). *Introduction to superconductivity*. Courier Corporation.
- Wang, H. Y., Ding, F. Z., Gu, H. W., Zhang, H. L., & Dong, Z. B. (2017). Microstructure and superconducting properties of $(\text{BaTiO}_3, \text{Y}_2\text{O}_3)$ -doped YBCO films under different firing temperatures. *Rare Metals*, 36(1), 37-41.
- Warembra, R. S., & Betaubun, P. (2018). Analysis of Electrical Properties Using the four point Probe Method. In *E3S Web of Conferences* (Vol. 73, p. 13019). EDP Sciences.
- Xu, Y., Hu, A., Xu, C., Sakai, N., Hirabayashi, I., & Izumi, M. (2008). Effect of ZrO_2 and ZnO nanoparticles inclusions on superconductive properties of the melt-processed $\text{GdBa}_2\text{Cu}_3\text{O}_{7-\delta}$ bulk superconductor. *Physica C: Superconductivity*, 468(15-20), 1363-1365.
- Yi, Y., Yu, X. F., Zhou, W., Wang, J., & Chu, P. K. (2017). Two-dimensional black phosphorus: Synthesis, modification, properties, and applications. *Materials Science and Engineering: R: Reports*, 120, 1-33.
- Yoshioka, D. (2012). Meissner effect cannot be explained classically. *arXiv preprint arXiv:1203.2227*.

- Yunus, N. E., Azman, N. J., & Jamion, N. A. (2018). Preparation and characterization of yttrium barium copper oxide (YBCO) superconductor with addition of cobalt oxide (CO_3O_4) *Journal of Academia*, 6(1), 31-38.
- Zhou, F., Ouyang, L., Zeng, M., Liu, J., Wang, H., Shao, H., & Zhu, M. (2019). Growth mechanism of black phosphorus synthesized by different ball milling techniques. *Journal of Alloys and Compounds*, 784, 339-346.
- Zhu, W., Kong, L., Long, W., Shi, X., Zhou, D., Sun, L., & Hou, X. (2021, April). Band Structure Engineering of Black Phosphorus/Graphene/ MOS_2 van der Waals Heterojunctions for Photovoltaic and Optoelectronic Device Application. In *Journal of Physics: Conference Series* (Vol. 1865, No. 2, p. 022021). IOP Publishing.

